CATO-2 Deliverable WP 3.3 - D12

Transport properties of intact caprocks and effects of CO_2-water-rock interaction

-

CO_2-induced mineral reactions in sandstone reservoirs

Prepared by: Mariëlle Koenen
Jan ter Heege
Rick Peeters

Reviewed by: Laura Wasch

Approved by: J.Brouwer
(CATO-2 Director)

1 Executive Summary (restricted)

A short- and long-term geochemical evaluation of CO_2 injection on the storage complex is required for EU regulations. The (site-specific) mineral reactions in a CO_2 storage reservoir and its caprock can be investigated by different methodologies. Experimental studies give insight in the true mineral reactions, providing that the right conditions are applied, but they are per definition short-term. For the long-term geochemical models are generally used which are able to extrapolate experimental results to longer time scales and can easily assess the effects of variations in mineralogical compositions of the rocks, as well as variations in e.g. pressure and temperature conditions, formation water composition and CO_2 partial pressure. However, these models are prone to significant uncertainties and they are per definition simple representations of the real, complex geological system.
In this deliverable we report on geochemical batch experiments combined with geochemical modelling to investigate the potential of these techniques for site evaluations. Rock material was selected from a potential storage site (the depleted gas field Barendrecht-Ziedewij) which was studied in detail in the natural analogue study within CATO-2 (Koenen et al., 2014). In that study, the Barendrecht-Ziedewij gas field was used as CO_2-free stratigraphic equivalent of a natural CO_2 reservoir, the Werkendam field. In the current study, sandstone material and low permeable clay-rich material from Barendrecht-Ziedewij was selected for batch experiments. Both powdered sample and rock cubes were reacted in a stainless steel high pressure vessel with brine at high temperature and CO_2 pressure for 4, 8 and 12 months to investigate CO_2 behavior in respectively a sandstone storage site and a clay-rich seal. The rock cubes were analysed by scanning electron microscopy after the experiment and compared to the unreacted sample, but no changes could be observed. For both sandstone and caprock, results of XRD analyses of the powder material, and ICP-MS analyses of the brine showed changes in mineralogy after the experiments. These changes do not show a clear evolution with time, possibly due to heterogeneity in initial mineralogy of the material, even though the powder was homogenized prior to the experiments. Yet, it was possible to deduce overall mineral reactions for the sandstone and the caprock. Subsequently, geochemical models were developed, which were fine-tuned to match the experimental observations as close as possible. The model results showed to be very sensitive to the input parameters selected, as well as to the assumptions made, showing the necessity of detailed petrographic and mineralogical characterization of the rocks for model development as well as careful interpretation of the results.

The results from this study show that geochemical batch experiments can help in the assessment of site specific gas-water-rock interactions. Powdering of rock material is required to increase the reactive surface area and enhance reaction kinetics. However, powdering of the rock destroys the rock textures which are crucial in the geochemical interactions. Careful interpretation of the experimental results is necessary and need support from petrographic analyses and geochemical modelling. Geochemical modelling, on the other hand, also requires careful interpretation since they are based on thermodynamic databases which are dealing with great uncertainties and oversimplified conditions. In addition, model results are sensitive to the selected input parameters and a thorough sensitivity analysis should be part of every geochemical assessment for a site evaluation.

Distribution List

(this section shows the initial distribution list)

External	Copies	Internal	Copies

Document Change Record

(this section shows the historical versions, with a short description of the updates)

Version	Nr of pages	Short description of change	Pages

Table of Content

2 Applicable/Reference documents and Abbreviations

2.1 Applicable Documents

(Applicable Documents, including their version, are documents that are the "legal" basis to the work performed)

	Title	Doc nr	Version
AD-01d	Toezegging CATO-2b	FES10036GXDU	2010.08.05
AD-01f	Besluit wijziging project CATO2b	FES1003AQ1FU	2010.09.21
AD-02a	Consortium Agreement	CATO-2-CA	2009.09.07
AD-02b	CATO-2 Consortium Agreement	CATO-2-CA	2010.09.09
AD-03h	Program Plan 2014	CATO2-WP0.A-D03	2013.12.29

2.2 Reference Documents

(Reference Documents are referred to in the document)

	Title	Doc nr	Version/issue	Date

2.3 Abbreviations

(this refers to abbreviations used in this document)

3 Introduction

A short- and long-term geochemical evaluation of CO_2 injection on the storage complex is required for EU regulations. This includes the behavior of CO_2 within the reservoir and its effect on caprock integrity.
In the Netherlands depleted gas fields are currently assessed as potential storage sites. In such storage reservoirs, only irreducible formation water is present. The reservoir can be considered as a closed system consisting of rock minerals and pore space filled with irreducible formation water (brine), supercritical CO_2 and a specific amount of remaining CH_4 after gas production. The main effect of the presence of CH_4 is the reduced partial pressure of CO_2, since CH_4 has a very low solubility in brine and hence geochemical effects are considered to be negligible (Tambach et al, submitted).
A caprock is part of the storage complex barrier. The caprock should have properties which prevent significant outward migration of CO_2 towards overlying aquifers or towards the surface (IPCC, 2005). This implies that the capillary threshold of the caprock should be high enough, or the CO_2 column small enough, not to allow darcy flow (Wollenweber et al, 2010, Busch and Müller 2011, Heat et al., 2012). If darcy flow does not occur, the only migration process would be slow, upward diffusion of dissolved CO_2. The capillary threshold of a rock is defined by its pore geometry, which is described by pore bodies (larger pore spaces between minerals grains) and pore throats (connections between the pore bodies along grain contacts) (Zhou and Stenby, 1993). The caprock of depleted gas fields has proven its integrity for methane storage on geological time scales. However, its integrity upon CO_2 storage needs investigation. CO_2 is known to lower the pH of the brine upon dissolution. With time, inward dissolved CO_2 might change the geochemical equilibrium of the caprock and initiate mineral reactions. These reactions are slow but on the longer term they might affect the pore geometry, and hence the sealing properties, of the caprock. These changes can either enhance the caprock integrity by clogging of the pore system, or decrease the integrity by widening of the pore throats.
Geochemical modeling results show that the gas-water-rock interactions depend on the initial mineralogy of the reservoir and caprock (Gaus et al., 2005). Therefore, case specific studies are required. During the last two decades many studies focused on the geochemical effects of injected CO_2 on the reservoir and caprocks. Short-term effects are important for injectivity, while long-term effects are important for geological containment and for (semi-) permanent trapping of the CO_2 in carbonates.

The (site-specific) mineral reactions in a CO_2 storage reservoir and its caprock can be investigated by different methodologies. Experimental studies give insight in the true mineral reactions, providing that the right conditions are applied, but they are per definition short-term. For the long-term geochemical models are generally used which are able to extrapolate experimental results to longer time scales and can easily assess the effects of variations in mineralogical compositions of the rocks, as well as variations in e.g. pressure and temperature conditions, formation water composition and CO_2 partial pressure. However, these models use thermodynamic databases containing mineral solubility data which are based on extrapolation of (short-term) experimental studies and hence they are prone to significant uncertainties (Dethlefsen et al., 2011). Furthermore, models are per definition simple representations of the real, complex geological system, which adds to the uncertainty in model output. Another way of investigating the complex geochemical reactions is by looking at natural CO_2 fields which represent natural analogues for CO_2 storage. These analogues can be used to calibrate or validate geochemical models. The three methodologies, experiments, modelling and natural analogue studies, are complementary, each of which having advantages and disadvantages.

Deliverable 28 of workpackage 3.3 reports on a natural analogue study which is representative for numerous potential storage locations in the Netherlands (Koenen et al., 2014). Mineralogical and petrographic analyses were performed to identify the mineral reactions which have occurred due to the presence of a high partial pressure of CO_2. In addition, geochemical modelling is performed to assess whether current modelling codes are able to predict the observed mineral reactions in the natural analogue and to investigate how much fine tuning is required. The results from this study indicated that mass transfer possibly occurred between the shaley intervals and the sandstone reservoir, as well as within the sandstones laterally. Hence, the storage complex was not a typical closed system to be represented by a relatively simple batch model. This is could be important to consider and will be further discussed later in this report.

This deliverable reports on the potential of geochemical batch reaction experiments in a case specific geochemical evaluation. It is based on the natural analogue study; we used sandstone and shale-rich rock samples from the CO_2-free, CH_4-bearing stratigraphic equivalent of the natural CO_2 reservoir with which the natural analogue was compared (Koenen et al., 2014). The batch reaction facility was developed within CATO-2. It allows the reaction of different materials at CO_2 storage conditions. Our aim is to provide semi-quantitative and qualitative information on the nature, the extent and the rate of reservoir and caprock alteration, and corresponding effects on mineral trapping in the reservoir and integrity of the caprock. The results are used to complement the natural analogue study and to validate and calibrate a PHREEQC geochemical batch model in the prediction of mineral reactions on the short term.

4 Experimental methodology

4.1 Introduction

The geochemical batch facility was developed at the beginning of CATO-2. Initially, it was used to evaluate cement alteration for the assessment of wellbore integrity. A detailed description of the development can be found in deliverable 12 of WP3.4.

4.2 Experimental facility

The facility consists of a 1 liter stainless steel 316L high pressure vessel with a reservoir of PTFE reinforced with glass fibre. The jacketed high pressure vessel is heated by heating oil, the temperature of which being controlled by a heated bath. (Figure 2). Inside the reservoir four separate PTFE holders are placed with rock material and brine inside. After closure of the vessel CO_2 is injected into the vessel to the desired pressure and the system is heated to the desired temperature. Thermocouples reaching into the pressure vessel and pressure measurement devices are placed on the cover of the pressure vessel and they are connected to a computer in order to monitor and record pressure and temperature of the $scCO_2$ during the experiments.

4.3 Material

A combined reservoir and caprock experiment was designed. Two holders were used for reservoir material, the other two for caprock material. Rock material from the Barendrecht-Ziedewij gas field was sampled. This field was selected based on the natural analogue study (Koenen et al., 2014). In this study samples of the natural CO_2 field Werkendam are compared to the CH_4 bearing stratigraphic analogue Barendrecht-Ziedewij to assess long-term mineral reactions induced by CO_2. Barendrecht-Ziedewij acts as a CO_2 free reference. By investigating mineral reactions on Barendrecht-Ziedewij experimentally, the results of the natural analogue study can be validated. Samples from reservoir and caprock were selected based on their composition (B1.10 and B1.2+B1.12 respectively). Part of the rocks were powdered in order to increase the reactive surface area of the material. Figure 3 shows the grain size distribution of the material after powdering. In addition, four rock cubes were prepared, two from the reservoir and two from the caprock (B1.12) sample (Figure 5).

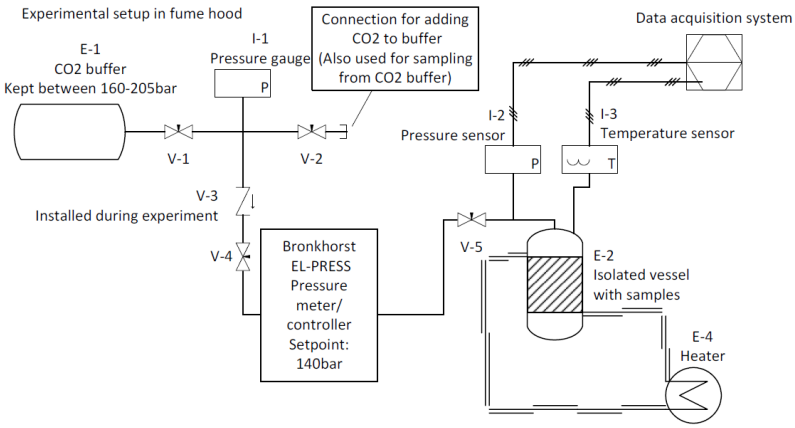

Figure 1. Schematic representation of the experimental set-up.

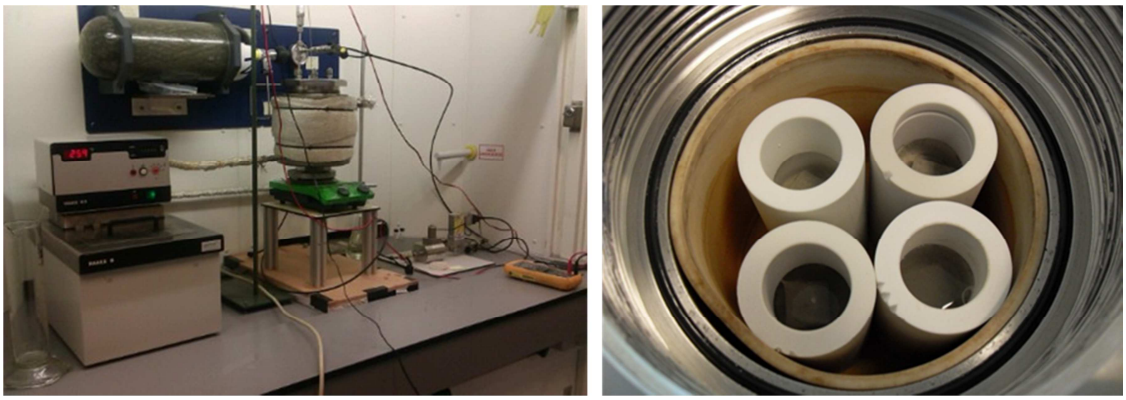

Figure 2. Left: Experimental set-up, consisting of a heated bath (left), a pressure vessel (right) and a CO_2 buffer (above the bath and the vessel). Right photo: the four reinforced PTFE holders inside the pressure vessel, containing powdered reservoir or caprock material, a rock cube and brine.

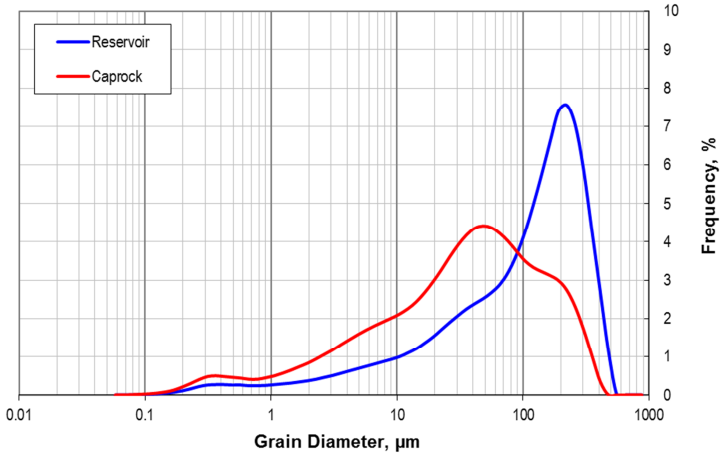

Figure 3. Grainsize distribution of the reservoir and caprock powder.

Table 1 Measured composition of Reedijk brine sample

Components	(mg/l)
Sodium (Na^+)	37,000
Potassium (K^+)	1,200
Calcium (Ca^{2+})	5,700
Magnesium (Mg^{2+})	1,300
Barium (Ba^+)	7
Strontium (Sr^{4+})	180
Iron (Fe^{2+} /Fe^{3+})	100
Chloride (Cl^-)	73,000
Sulphate (SO_4^{2-})	500
Bicarbonate (HCO_3^-)	180

A synthetic brine was made, based on a brine sample from the same lithological unit of the Reedijk field which is located near Barendrecht-Ziedewij (Table 1). The components of the simplified synthetic brine are shown in Table 2. Iron was left out of the brine since addition of a tiny amount of $FeCl_2$ would cause the formation of yellow/orange precipitates. Barium and strontium are not included as well. Table 3 shows the concentrations of the major ions in the brine based on the composition in Table 2, and two measured samples from two different brine batches. The measured concentrations of S and Cl are semi-quantitative. The prepared and measured concentrations are similar but show slight deviations which can be assigned to inaccuracies in measured components during preparation and inaccuracies in ICP-MS measurements.

Table 2. Components of the synthetic brine.

Components	(mg/l)
NaCl	90,000
$CaCl_2$	15,000
MgCl2	4,800
K_2SO_4	800
KCl	1,400

Table 3. Concentration of major ions in mg/l as intended, based on the composition as shown in Table 2 (sample prepared) and measured in two samples from two different brine batches.

	Sample as prepared (mg/l)	Sample measured (mg/l)	Sample measured (2) (mg/l)
Na	35415	32350	31440
Cl	68408	68040	60240
Ca	5417	5023	4727
Mg	1225	1081	1104
K	1093	1341	986
S	147	0	0

4.4 Experimental design

Four holders are placed inside the vessel. In each holder 23.5 gram of powder material is inserted, with a rock cube of 6.7 gram on top. Subsequently, 21.6 gram of brine is added thereby completely submerging the cubes (Figure 2). This results in a rock/brine ratio of 1.4 by weight. Each holder represents a separate system, thereby assuming that supercritical CO_2 ($scCO_2$) does not allow diffusion of ions. After four months the experiment was stopped, pressure and temperature were slowly lowered to atmospheric conditions and the vessel was opened. One of the holders with caprock material was removed and the material was prepared for analysis. Subsequently, the holder was prepared with new caprock powder and the cube from the four-months experiment and placed inside the pressure vessel. The vessel was closed and the experiment was started again. After another eight months, the experiment was terminated. At this point we had powdered material which reacted for 4, 8 and 12 months allowing us to develop a time series of the results. The four cubes have reacted for 12 months.

4.5 Sample preparation, characterization and data analysis

4.5.1 Sample preparation

After the experiment the brine in the holders was cloudy (Figure 4). The holders were covered and left to settle for about 30 minutes. Then, for each holder two times 3-5 ml of brine was pipetted with a needle pipet and injected into two small glass bottles. Some suspended material might have been entrained during pipetting. Leaving the brine in the glass bottles for a few hours results in precipitates at the bottom of the bottles (Figure 4). From each set, one bottle is prepared for an ICP-MS sample from the bulk of the brine (turbid brine), from the other bottle an ICP-MS sample is taken from the clear brine after settling of the precipitates for a few hours.
The remaining material in the holder was poured into a funnel with a filter paper cup inside (Whatman™ 10311645 Grade 595½ Prepleated Cellulose Qualitative Filter Paper, 4-7µm mesh) (Figure 4). If sufficient brine was left, the brine was intercepted in a bottle below the funnel (Figure 4). Subsequently the powder was washed in the filter cup using a pre-defined amount of filtered, deionized water (milli-Q). The milli-Q water ('washing' water) was intercepted in a new bottle below the funnel. The rock cubes, which had turned bright red at the top (Figure 5), were placed in demi-water for 1 day to remove salts from the brine in the pores. Of both the filtered brine, the washing water from the powder and the leaching water of the cubes samples were prepared for ICP-MS.
We realize that there is a risk that precipitates formed in the brine as a result of cooling. The results from the different ICP-MS samples per holder might give the opportunity to distinguish between particles and precipitates. After washing of the powder and leaching of the cube, the material was put in PTFE cups and placed in a 40°C oven for drying for 2-3 days. Subsequently, the dry powder material was send to Qmineral in Leuven, Belgium, for detailed XRD analysis. The rock cubes were send to the British Geological Survey for thin section preparation.

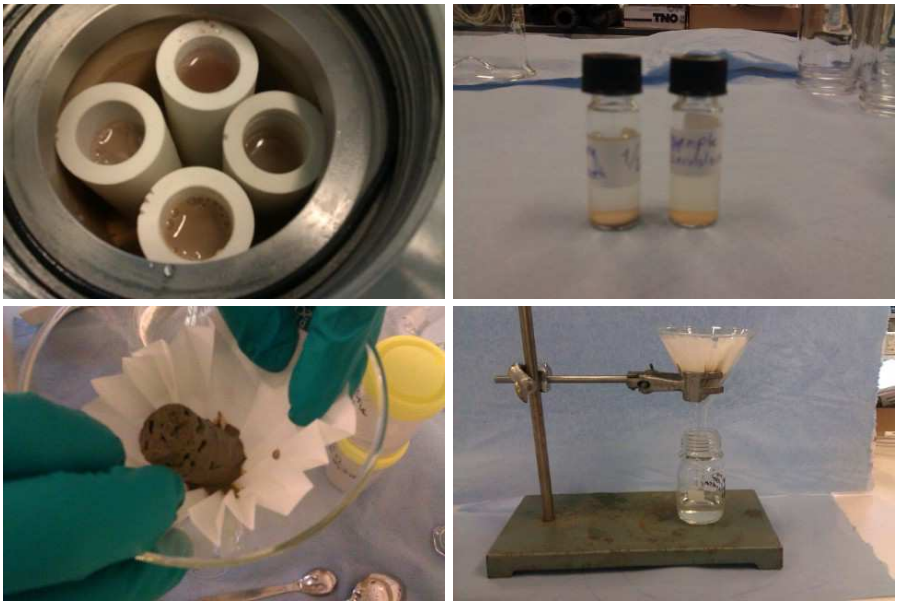

Figure 4. Upper left: The brine is cloudy after the experiment. Upper right: two glass bottles with brine pipetted with a needle pipet from the holders. Note the settling of suspended material at the bottom. Lower left: the wet powder material is put in a funnel with a paper filter. Lower right: brine is intercepted in a bottle below the funnel.

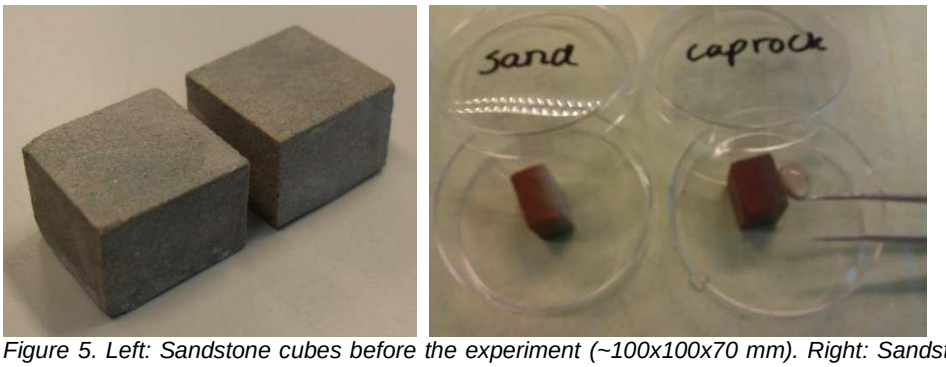

Figure 5. Left: Sandstone cubes before the experiment (~100x100x70 mm). Right: Sandstone and caprock cube after the experiment. The top of the cubes has turned red.

4.5.2 Reservoir and caprock characterization

Characterization of reference material (before reaction) and samples used during the experiments was performed using several analytical techniques. Detailed whole rock and clay fraction X-ray diffraction (XRD) was performed by Qmineral in Leuven, Belgium of untreated samples and reacted powder samples.
Thin sections were prepared from reference material and from the rock cubes after reaction. These thin sections were analysed for petrographic analysis using Scanning Electron Microscopy (SEM) equipped with the following detectors:

- Backscattered Electron (BE) detector: The BE detector can make images which can be used to see chemical differences (lighter colour means heavier elements)
- Energy Dispersive X-rays (EDX) for a semi-quantitative chemical analysis. EDX was used for element distribution maps and chemical cross sections.

4.5.3 Brine analysis

Fluid analyses have been performed by ICP-MS on brine and washing water. This technique measures the concentration of a range of metals and non-metals, even at very low concentrations. These analyses were performed at TNO. The concentrations of Si, S and Cl are semi-quantitative.

5 Results

5.1 Reservoir and caprock mineralogy - XRD

Figure 6 and Figure 7, and Table 4 and Table 5 show respectively the whole rock and clay fraction mineralogy of the reservoir and caprock material initially and after 4, 8 and 12 months of reaction. Whole rock XRD analysis on the unreacted material shows that the reservoir rock consists mainly of quartz (64.5%), anhydrite (13.5%) and alkali feldspar (9.7%). The remaining mineralogy is made up of plagioclase (albite), 2:1 aluminium rich silicates (clay minerals), kaolinite, dolomite and siderite. The caprock material consists mainly of quartz (43.7%) and 2:1 aluminium rich silicates (clay minerals, 34%). The remainder is made up of alkali feldspar, plagioclase (albite), kaolinite, siderite, dolomite, anatase and halite. The clay fraction of the reservoir and caprock is similar, consisting of kaolinite, illite and illite/smectite, but the amount of kaolinite is much higher in the reservoir rock and hence, the amount of illite and illite/smectite mixed layers is lower. The grain size distribution indicates that the clay fraction makes up a larger part in the caprock than in the sandstone material, and hence the absolute amount of kaolinite is probably higher (Figure 3). The amount of kaolinite in the whole rock analyses is also higher in the caprock. The ratio of illite to smectite in the mixed layers is approximately 83 : 17 for both reservoir and caprock.

After reaction the analyses show slight differences in mineralogy. These differences do not show a clear evolution with reaction time for both the reservoir and the caprock. A possible explanation is that the powder material was not homogenised well and any disturbance in the trend is the result of initial heterogeneity of the material. For the reservoir rock, the mineralogy of the sample

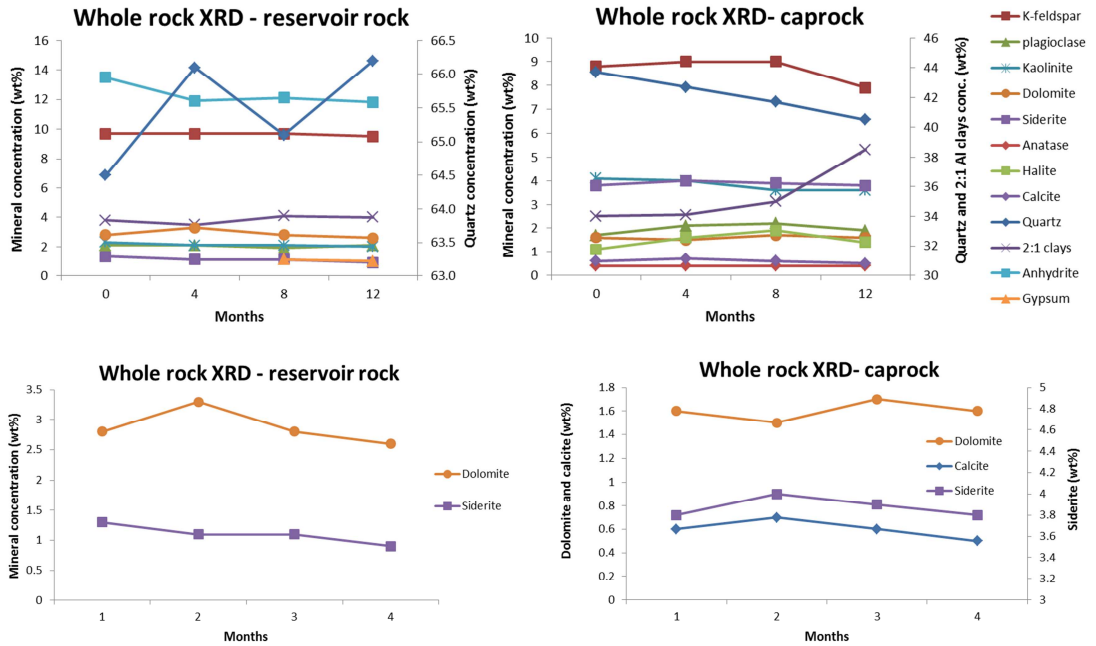

Figure 6. Diagrams from the XRD results for the whole rock analyses. Upper graphs: all minerals. Note that both diagrams have a secondary y-axis for quartz and/or 2:1 Al clays. Lower graphs: results for the carbonates only.

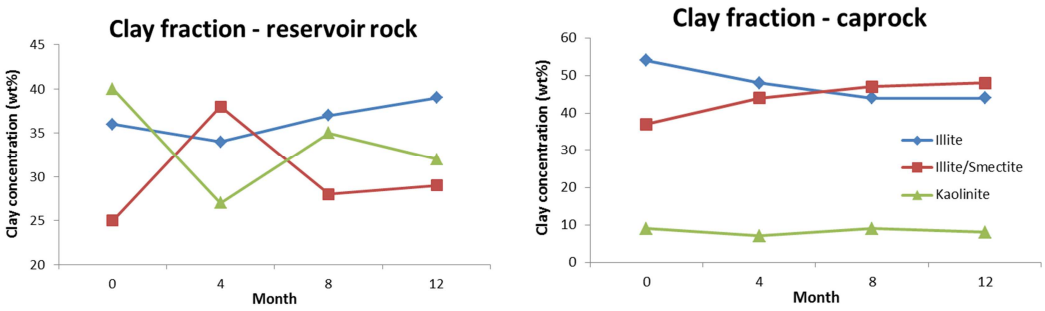

Figure 7. XRD results for the clay fraction analyses (grains < 2µm).

Table 4. XRD results for the whole rock analyses.

	Sandstone				Caprock			
Mineral	**Initial**	**month 4**	**month 8**	**month 12**	**Initial**	**month 4**	**month 8**	**month 12**
Quartz	64.5	66.1	65.1	66.2	43.7	42.7	41.7	40.5
Alkali feldspar	9.7	9.7	9.7	9.5	8.8	9.0	9.0	7.9
Plagioclase	2.1	2.1	1.9	2.1	1.7	2.1	2.2	1.9
2:1 Al sheet silicates	3.8	3.5	4.1	4.0	34	34.1	35	38.5
Kaolinite	2.3	2.1	2.1	2.0	4.1	4.0	3.6	3.6
Calcite					0.6	0.7	0.6	0.5
Dolomite	2.8	3.3	2.8	2.6	1.6	1.5	1.7	1.6
Siderite	1.3	1.1	1.1	0.9	3.8	4.0	3.9	3.8
Anhydrite	13.5	11.9	12.1	11.8				
Gypsum			1.1	1.0				
Anatase					0.4	0.4	0.4	0.4
Halite					1.1	1.6	1.9	1.4

Table 5. XRD results for the clay fraction analyses (grains < 2µm).

	Sandstone				Caprock			
Mineral	**Initial**	**month 4**	**month 8**	**month 12**	**Initial**	**month 4**	**month 8**	**month 12**
Illite	36	34	37	39	54	48	44	44
Illite/Smectite	25	38	28	29	37	44	47	48
Kaolinite	40	27	35	32	9	7	9	8

which reacted for 4 months shows some disturbance in the trends, concerning the concentration of quartz, dolomite, 2:1 Al clay minerals and the minerals identified in the clay fraction analyses. Overall, the following reactions can be observed for the reservoir rocks: dissolution of dolomite and siderite, and reaction of kaolinite to illite, illite/smectite and quartz. Anhydrite dissolution and

partial conversion to gypsum can be observed. Note that the changes are very small, and that the trends are not statistically justified. The changes in the caprock samples show some trends with increased reaction time: small amounts of alkali feldspar, quartz and kaolinite react to form 2:1 Al clay minerals, and illite partially converts to illite/smectite.

5.2 Fluid analyses

Sampling techniques

For both the reservoir rock and the caprock material ICP-MS analysis is performed on the following brine samples after 4, 8 and 12 months:

- Clear brine (pipetted off, after settling)
- Turbid brine (pipetted off, before settling)
- Filtered brine (remaining brine through filter after pipetting)
- Washing water ('washing' of powder through filter)
- Leaching water (leaching of cubes, only after 12 months)

The results of the ICP-MS analysis in absolute values are shown in Appendix A and Appendix B. Table 6 and Table 7 show the change in concentration with respect to the initial brine composition for reservoir and caprock respectively.
Washing of the powder material and leaching of the cubes allow the cations in the pore water to be removed from the solid material to prevent precipitation upon drying. However, additional reactions might occur when the sample material gets in contact with fresh water. Chlorine is generally not involved in any reaction. The concentrations of the filtered, clear and turbid brine were divided by the concentrations in the washing water and the leaching water (Appendix C). Comparing the ratio of the elements to the ratio for chlorine provides insight in the additional reactions upon washing and leaching.

Each of the brine sampling techniques (filtered, clear or turbid) has advantages and disadvantages and it is not clear which of these is most representative for the real brine composition. During filter and pipetting of the brine from the holders, powder material might have been entrained. Since the finest powder is most likely to be entrained, and the finest powder consists of clay minerals, high concentrations of aluminium in the samples could indicate the inclusion of powder material in the ICP-MS samples. The results show that the Al concentrations are overall very low, often below detection limit. A few measurements might point to clay entrainment (values in green in Appendix A). The excess amounts of Al all occur in turbid brine.
The differences between the three brine sampling types are significant, though not consistent, and hence the results only allow interpretation on a general level. Considering the issues with regard to the pipetting of the brine from the holder, whereby varying amounts of powdered material might be entrained, the trends in the filtered brine are probably most reliable.

Effect of evaporation

The concentrations of Na and Cl increase with time for both the reservoir and caprock experiments. Sodium can be involved in mineral reactions like albite dissolution or precipitation or adsorption/desorption on clay surfaces. The Cl increase, on the other hand, suggests a continuous, gradual evaporation of water with time, since Cl is not a common constituent of minerals except for halite. Halite was not identified in the reservoir samples, while some halite was observed for the caprock samples (Table 4). The increased halite concentration in the caprock samples after the experiments would result in lower NaCl concentrations in the brine if evaporation had not taken place. Hence, for both the reservoir and the caprock we can conclude that evaporation must have occurred. The increase in concentration of the other elements could also be (partially) due to the evaporation of water. To assess the potential influence of

evaporation, all values are divided by their original value in the initial brine to obtain normalized values for comparison with the 'evaporation factor' for Na and Cl (Appendix D).

5.2.1 Reservoir experiments

The ICP-MS results show increased concentrations with respect to the initial composition for all elements after the experiments (Table 6 and Appendix B). In Figure 8 the normalized concentrations (measured concentration after the experiment divided by initial concentration) of several major elements are plotted with time. For Al, Si, S and Fe, the initial brine concentration was below detection limit and hence, normalized values cannot be calculated. The major elements show a general increase in concentration with time. The 'evaporation factor' (measured Na or Cl concentration after the experiment divided by their initial concentration) for both Na and Cl are ~1.0, 1.3 and 1.5 after 4, 8 and 12 months respectively (Figure 8), corresponding to a continuous water evaporation with time.

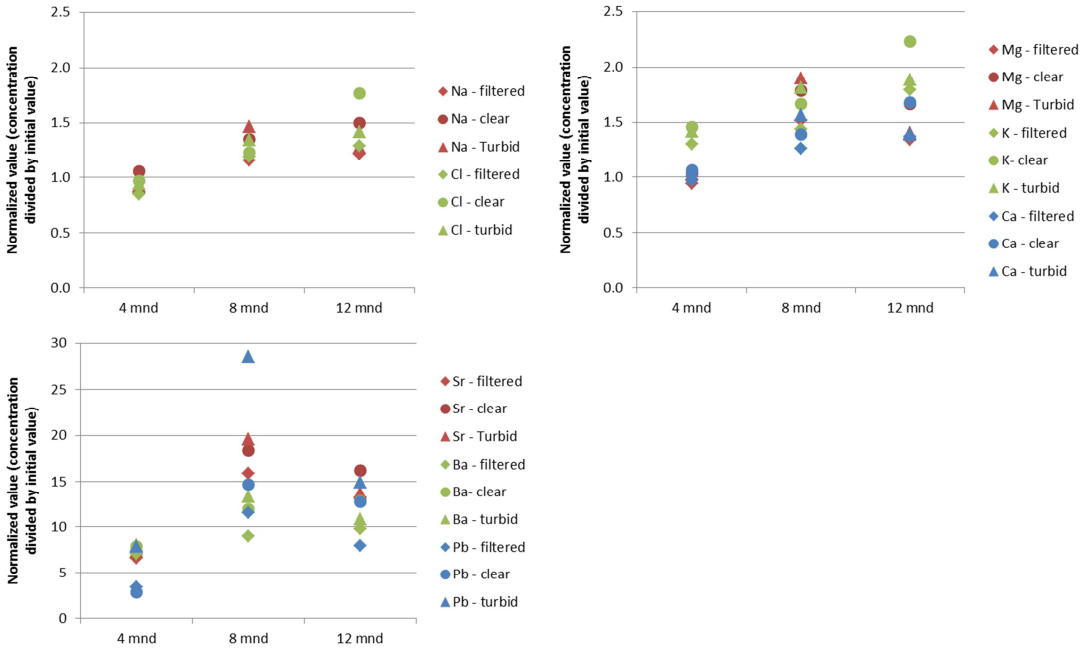

Figure 8. Reservoir rock experiment. The concentrations of several major and trace elements are divided by their initial concentration.

The normalized values for Mg and K are slightly higher than the evaporation factors for Na and Cl, suggesting that their increased concentrations are only to a small extent the result of mineral dissolution. The normalized values for Ca are not significantly higher than the values for Na and Cl. In addition to the increased K normalized concentration, the increased Ba and Pb values suggest dissolution of K-feldspar (Figure 8). Barium and to a lesser extent Pb are common impurities in this mineral in which they substitute for K (De Vos and Tarvainen, 2006). The slight Mg increase could indicate dissolution of dolomite while this is not supported by the Ca concentrations. In addition, the low Ca values do not suggest anhydrite dissolution, even though the anhydrite (+ gypsum) content from the XRD analysis is lower for each of the experiments than the initial value. The increased Sr concentration suggests either dolomite or anhydrite dissolution

*Table 6. The Δ in brine composition in mg/l wrt the initial brine in mg/l for the reservoir experiments. The washing and leaching water are excluded. *values in µg/l.*

		Li*	Na	Mg	Al	Si	S	Cl	K	Ca	Mn*	Fe	Co*	Ni*	Cu*	Zn*	Sr*	Ba*	Pb*
4 months	filtered brine	1650.5	-4494.5	-63.4	1.3	175.9	-	-8879.1	296.4	-129.9	3343.6	100.2	-0.1	19002.1	331.1	80422.2	15519.4	1831.6	147.0
	Clear brine	1788.7	1826.4	38.9	1.9	190.6	-	-1843.7	450.9	299.0	3653.5	90.2	-0.1	23403.3	392.1	92371.4	17299.2	2075.2	113.1
	turbid brine	1746.9	-2348.7	33.8	8.5	220.1	-	-3488.2	413.8	279.8	3765.0	153.6	-0.1	21181.7	692.7	95533.8	17407.2	2121.4	423.0
8 months	filtered brine	3394.9	5140.0	559.9	-	167.4	542.3	12808.0	581.3	1334.0	-	-	190.8	1328.7	2645.4	7247.3	43281.3	2282.5	380.1
	Clear brine	3473.1	11322.3	848.9	-	194.6	-	15816.8	885.7	1957.3	-	-	220.8	1558.3	3145.8	8818.3	50389.7	3104.4	493.1
	turbid brine	3941.4	14918.6	971.9	-	235.4	-	23187.8	1084.0	2823.2	-	55.7	241.2	1676.7	3384.5	10249.0	53759.4	3509.8	992.1
12 months	filtered brine	2784.3	6806.1	377.5	-	221.1	577.3	17653.4	775.8	1751.7	2285.5	38.4	205.7	783.1	1274.7	4476.9	33885.0	2650.0	430.1
	Clear brine	3544.3	15677.9	730.8	-	297.3	785.5	45818.7	1212.2	3205.7	2605.4	45.2	269.8	1067.2	1820.9	6184.4	42168.1	3570.1	725.2
	turbid brine	2801.9	8712.8	447.1	-	240.4	-	24911.1	867.7	1839.0	2675.0	60.9	232.2	1300.2	1478.3	5555.6	35318.3	2961.7	854.2

*Table 7. The Δ in brine composition in mg/l wrt the initial brine in mg/l for the caprock experiments. The washing and leaching water are excluded. *values in µg/l.*

		Li*	Na	Mg	Al	Si	S	Cl	K	Ca	Mn*	Fe	Co*	Ni*	Cu*	Zn*	Sr*	Ba*	Pb*
4 months	filtered brine	-	-	-	-	-	-	-	-	-	-	-	-	-	-	-	-	-	-
	Clear brine	7687.7	10469.7	685.5	1.6	103.2	-	23795.0	763.7	1952.7	2102.9	25.7	-0.1	1281.8	1968.9	11018.6	23943.8	2266.4	5588.2
	turbid brine	8084.6	11758.4	812.9	138.3	381.9	-	24030.2	858.8	2207.5	4894.0	270.8	-0.1	1894.3	2253.1	17182.8	26109.6	3110.2	12012.1
8 months	filtered brine	6751.5	951.1	326.5	-	166.2	-	-7443.8	317.7	356.0	-	32.2	63.6	1377.2	1018.2	13563.3	21241.6	2134.7	6312.3
	Clear brine	8000.1	7252.7	584.8	-	193.8	-	8424.3	618.2	1341.6	-	35.1	68.2	1793.0	1286.5	17123.8	25337.0	2702.4	8128.0
	turbid brine	6980.1	2471.2	388.2	-	179.0	-	64.4	385.2	609.4	-	57.2	71.3	1546.9	1142.3	14991.0	22237.0	2390.6	9423.9
12 months	filtered brine	11688.7	12266.0	954.6	-	181.0	-	22990.0	659.7	3354.1	2187.6	-	131.5	2141.7	2944.8	16329.3	52251.0	2983.3	5346.4
	Clear brine	11376.5	11190.0	903.2	-	182.0	-	23015.5	582.0	3077.4	2060.7	-	138.2	2159.0	2901.8	16428.2	50193.5	2952.4	5934.3
	turbid brine	12102.0	14077.1	1032.6	8.4	208.8	-	27644.4	717.5	3511.3	2297.1	50.7	144.3	2267.8	3164.1	19358.0	54014.5	3211.5	7648.9

(Figure 8), since Sr is a common impurity in these minerals, in which it is substituted for Ca (De Vos and Tarvainen, 2006, Jacobson and Usdowski, 1976, Kramm and Bless, 1986). The trend for Sr follows the trend for Mg in time better than the trend for Ca, suggesting that the Sr is mainly partitioned in dolomite and not anhydrite. The S concentrations are variable, but mostly below detection limit (Table 6) and hence, the measurements seem unreliable.
Barium, Pb, Zn, Cu and Fe show increased concentrations as well. These elements are closely associated with clay minerals (De Vos and Tarvainen, 2006). These elements were probably liberated through desorption or cation exchange with sodium during the experiment. Dissolution of the clay minerals did not occur since Al concentrations are low to negligible (Appendix A).

The washing and leaching water have much lower element concentrations than the brines (Appendix A), as expected. If the washing water and leaching water would only 'sample' the brine which is left behind in respectively the powder material and the rock cube, the ratio of the concentration in the filtered, clear or turbid brine to the concentration in the washing or the leaching water (Appendix C) would be similar for all elements. The values for S, Ca, Mn and Sr show lower values, suggesting additional anhydrite dissolution from the powder material and especially from the rock cubes. Barium, Pb, Zn, Cu and Fe values are high, suggesting re-adsorption onto, or cation exchange in clay minerals. These elements, which were probably liberated through desorption or cation exchange with sodium during the experiment might have been adsorbed or exchanged again when the clay minerals got in contact with the fresh washing or leaching water. The adsorption, desorption and/or cation exchange reactions could not have affected the XRD analyses since these reactions do not involve mineral changes.

5.2.2 Caprock experiments

The ICP-MS results show increased concentrations with respect to the initial composition for all elements except sulphur after the experiments (Table 7 and Appendix B). In Figure 9 the normalized concentrations of several major and trace elements are plotted in time. Like for the reservoir brine, for Al, Si, S and Fe, the initial brine concentration was below detection limit and hence, normalized values cannot be calculated. The samples from turbid brine after 4 and 12 months experiment show excess Al and high Si, Fe and Pb concentrations suggesting the entrainment of clay powder. For these samples Ca, Mg and K and other trace elements but Pb do not show deviating values, suggesting that these elements are not linked to the aluminium rich clays in this rock sample.
The trends for Na, Cl, Ca and Mg with time are very similar and show an increase in concentration after 4 months, a decrease after 8 months, and an increase after 12 months to values exceeding the 4 months experiment. This is due to a difference in evaporation, which was significant in the 4 months experiment and small in the 8 months experiment (Appendix A).The slightly higher normalized values for Ca and Mg, compared to those for Na and Cl, suggest a continuous dissolution of dolomite. The closely correlated increase in Ca and Mg concentrations suggest that significant calcite dissolution did not occur. The increase in Sr concentration with time supports the continuous dissolution of dolomite. The increase in K concentration is small but the increased Ba and Pb normalized values do support some dissolution of K-feldspar. Increased concentrations of Fe, Ni, Cu, Zn and Co (and Pb) suggest desorption from clay minerals and or cation exchange with Na from the brine.

As for the reservoir experiments, the washing and leaching water have much lower element concentrations than the brines (Appendix A). Considering that Na and Cl represent more or less the brine composition in the powder material and the rock cubes, several elements have significantly lower concentrations in the washing water and leaching water (Appendix C). In the leaching waters, this is especially true for Mg, Ca and Sr (and Ni), which are representative for dolomite. Ni could be associated to dolomite, but also to clays, in the other samples, Ni does not

have significantly deviating values. Possibly, dolomite has precipitated when the acid brines were mixed with fresh water. In the washing waters, especially Fe, Cu, Zn, and Pb have low concentrations. These are associated with clay minerals. Like for the reservoir experiments, these elements, which were probably liberated through desorption or cation exchange during the experiment (the clay minerals are not dissolved since Al concentrations are low) might have been adsorbed or exchanged again when the clay minerals got in contact with the fresh washing or leaching water.

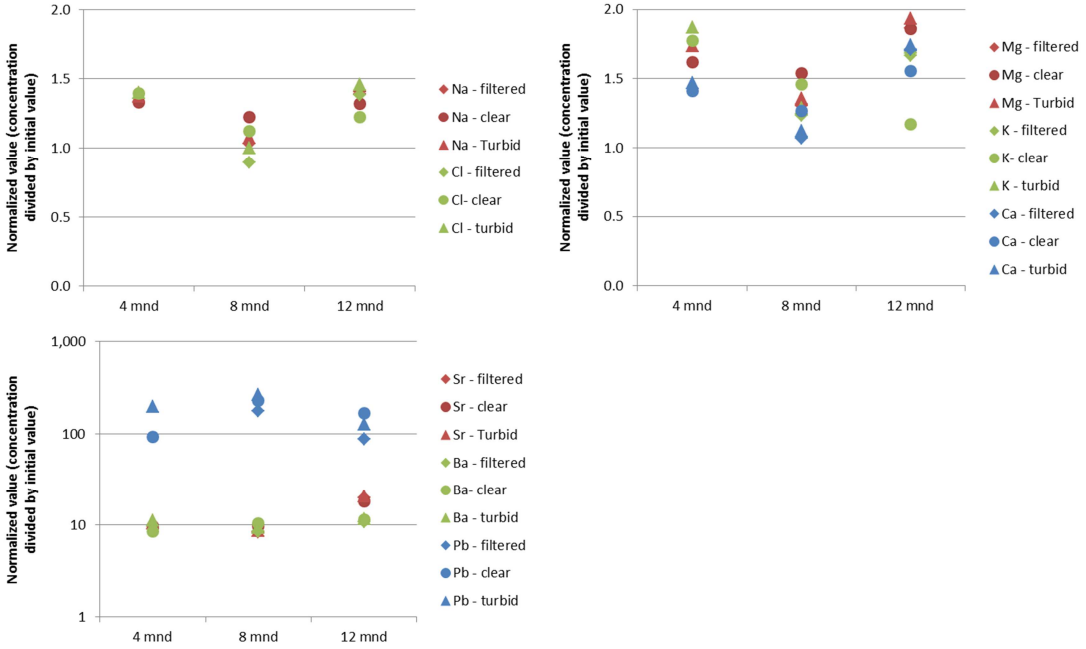

Figure 9. Caprock experiment. The concentrations of several major and trace elements are divided by their initial concentration. Note the logarithmic scale for the bottom graph.

5.3 Petrographic analysis

The thin sections of the reacted rock cubes were investigated for changes in microscopic characteristics. We looked for dissolution features on minerals and secondary mineral precipitates which were not observed in the unreacted rocks.

5.3.1 Reservoir rock

The Barendrecht-Ziedewij reservoir rock is studied in detail in CATO-2 and reported in D28a (Koenen et al., 2014). In this section a summary is given.
The dominant detrital mineral within the Barendrecht-Ziedewij sandstones is quartz. The detrital quartz grains have a rounded or elongated shape. K-feldspar is the most common type of feldspar while detrital albite is rare. Most K-feldspars are partially albitized and they show dissolution along cleavage planes and/or have corroded rims. The dominant micas are muscovite and biotite. Detrital mica is often deformed or squeezed between K-feldspar or quartz grains. Biotite and occasionally muscovite are partially replaced by authigenic minerals. Authigenic

kaolinite is the main clay mineral present within the samples, apart from (primary) illite in clay clasts. Vermicular type of kaolinite occurs either as an alteration product of K-feldspar (Figure 11) and mica (mainly biotite, occasionally muscovite), or within the intergranular pore space. The kaolinite resulting from K-feldspar dissolution occasionally fills up the secondary pore space. The kaolinite in primary pores is present as booklets. Occasionally, the larger booklets show alternating crystals of kaolinite and either illite or biotite/muscovite (iron and magnesium content is between biotite and muscovite end-members). From the morphology and size, it seems to be mica. These mica layers are rich in K with significant amounts of Mg and Fe. These features can be interpreted as mica (either Mg-Fe rich muscovite or Mg-Fe poor biotite) alteration to kaolinite and illitization of kaolinite. Kaolinite is either the result of mica alteration or is a product of K-feldspar leaching.

Zoned dolomites are abundant with two, maximally three growth zones. In total 5 different types of siderite have been recognized based on their morphologies and association (Figure 11). When kaolinite replaces biotite, it is often associated with anhedral, granular siderite crystals. Siderite with the same morphology is also abundant within clay clasts (sid 2). The zoned dolomites are often surrounded by small patches of siderite (sid 3). The siderite probably represents a different phase than the siderite nodules associated with mica alteration and clay clasts. The patches are small and contain micropores. Also larger, pore-filling siderite cement (sid 4) can be observed which replaces earlier authigenic quartz. In addition, euhedral siderite grains forming aggregates (sid 5), are observed which have grown adjacent to, or replaced quartz overgrowth.
The most common and extensive cement is anhydrite. It forms large patches of blocky, poikilitic, pore-filling cement. It encloses intragranular kaolinite within residual K-feldspar grains (Figure 11), indicating K-feldspar alteration to kaolinite prior to anhydrite cementation. Anhydrite also encloses siderite (sid 3), which in turn encloses dolomite (Figure 11).
After reaction, the petrographic analysis did not result in clear changes in microstructural characteristics with the unreacted samples. Dissolution edge pitches can be observed in the anhydrite but it is not clear whether these actually formed during the experiments. In the unreacted rocks, anhydrite has generally less dissolution pitches, but in some samples, the anhydrite is highly irregular in shape, showing dissolution and/or broken features from thin section preparation. Two geochemical cross sections were developed using SEM EDX by analysing large surface areas (~1.7 mm^2 which is sufficiently large to prevent the effect of heterogeneities) in

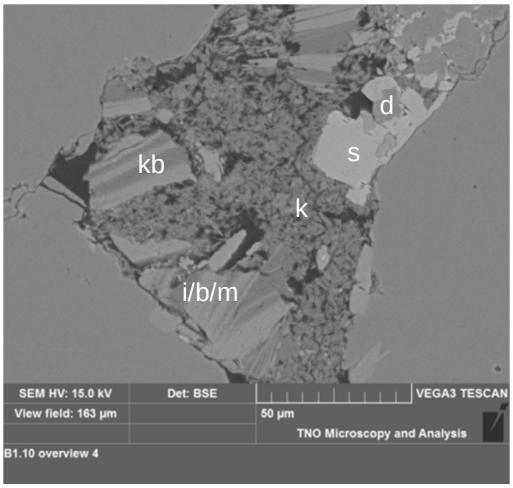

Figure 10. Fine grained kaolinite (k) and large kaolinite booklets (kb) with alternating illite or biotite/muscovite (i/b/m). Dolomite (d), enclosed by siderite (s).

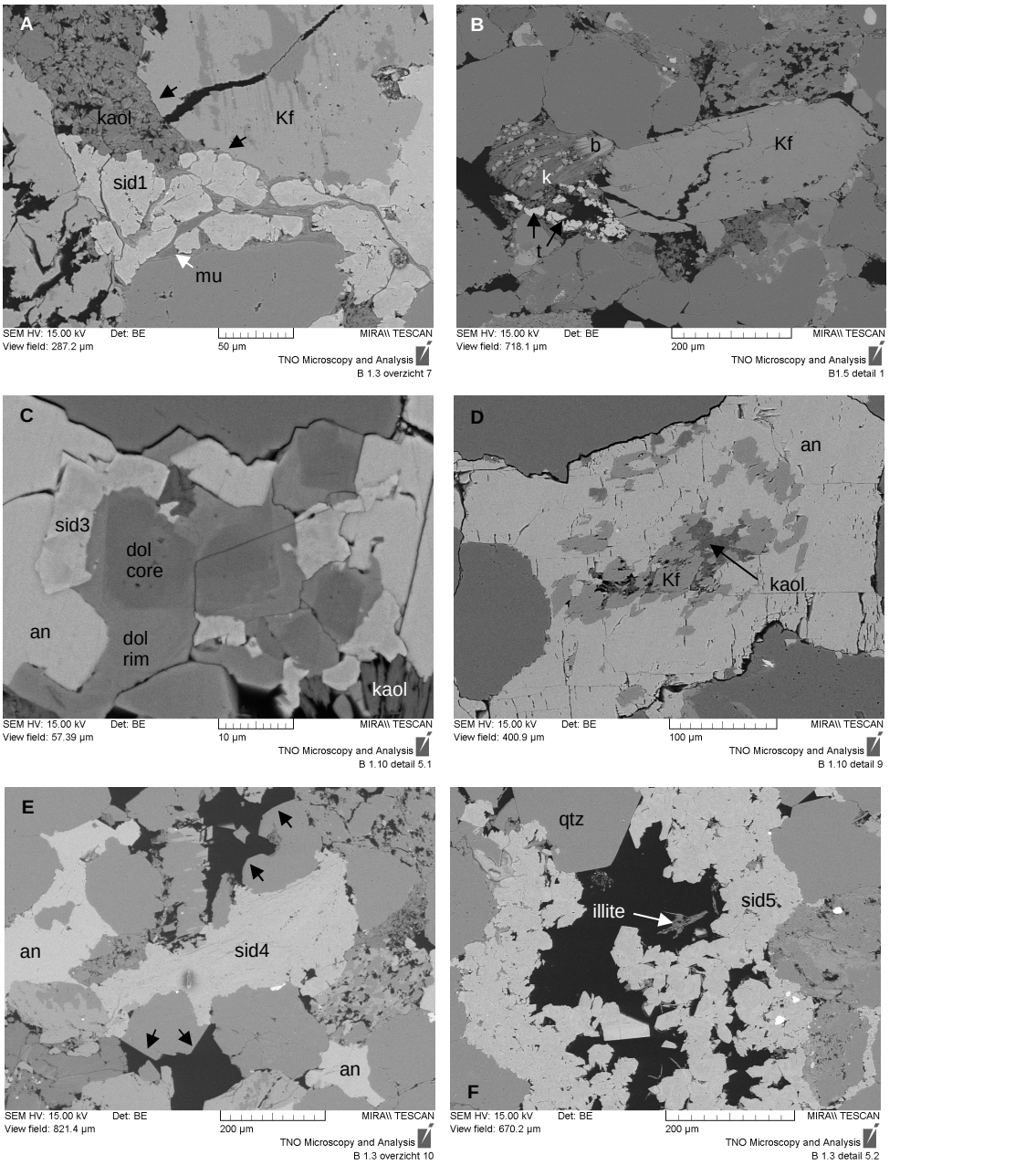

Figure 11. SEM BSE images of BRTZ samples. A:Partially albitized K-feldspar grain. The albitized zones terminate against K-feldspar overgrowth (black arrows). A fracture runs right through the grain, including the overgrowth. Almost complete replacement of muscovite (mu) by (partially intergrown) kaolinite and siderite (sid 1). B: Fractured K-feldspar grain with overgrowth. Biotite flake (b) replaced by kaolinite (k) and anhedral siderite nodules (sid 1). Right below, kaolinite with authigenic Ti-oxide (t). C: Zoned dolomites (dol), surrounded by siderite (sid 3) and anhydrite (an). D: K-feldspar (Kf) alteration to kaolinite (kaol), secondary pore space cemented by anhydrite. E: Pore-filling anhydrite (an) and siderite cement (sid 4). Siderite replaces quartz overgrowth (black arrows). F: Euhedral siderite aggregate (sid 5) intergrown with fibrous illite, growing adjacent to, or replacing quartz overgrowth.

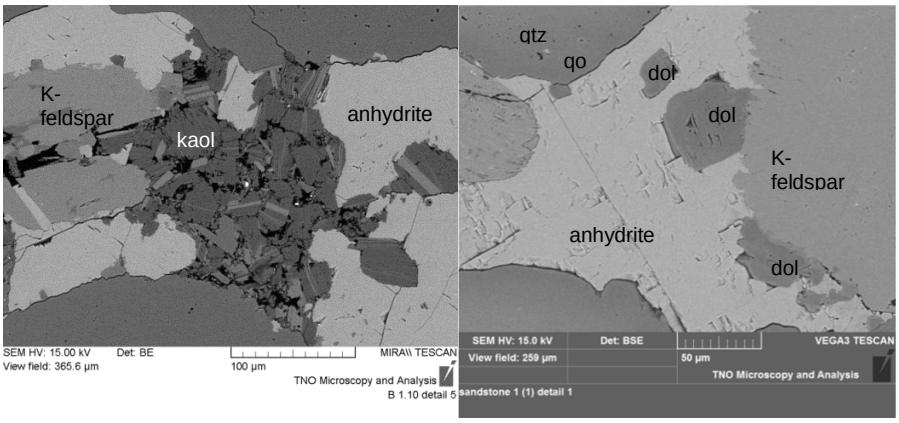

Figure 12. Left: anhydrite cement prior to reaction with limited dissolution pitches. Right: anhydrite cement after reaction with many dissolution pitches.

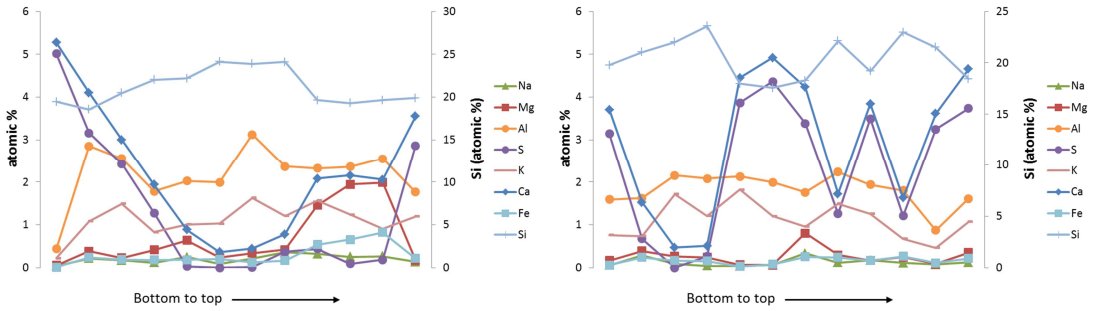

Figure 13. Geochemical cross sections from bottom to top. Each measurement represents a surface area of ~1.7 mm^2. All elements shown except for oxygen. Note that silica is shown on the right axis.

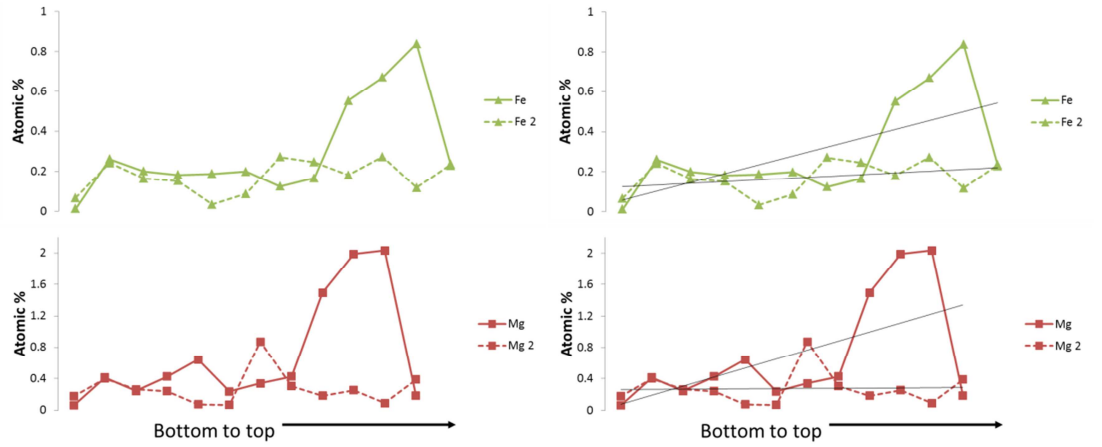

Figure 14. Compilation of two cross sections for iron (Fe and Fe-2) and magnesium (Mg and Mg-2). These values are based on EDX analyses normalized excluding carbon, calcium and sulphur since carbon is biased by the epoxy and . calcium and sulphur are highly variable due to local anhydrite cementation. The right diagram includes trendlines. One of the cross sections shows iron and magnesium enrichment towards the top, the other does not show a trend.

sequence from bottom to top by EDX. The results are shown in Figure 14. Note that carbon was not included in the quantification since the thin sections prepared from the reacted cubes were impregnated with carbon-containing epoxy. The large heterogeneity in calcium and sulphur content, which are clearly related, reflect the initially present local anhydrite cementation. The silica content shows a negative correlation with calcium and sulphur. The other elements are more stable over the sections. In Figure 14 the cross sections are blown up for iron and magnesium to investigate potential redistribution within the samples. These elements are incorporated in the carbonates (siderite and dolomite). Upon oxidation, iron becomes more mobile and hence, migration and subsequent precipitation of iron oxides might explain the red coloration of the cubes. Trendlines are added in the graphs on the right. For one of the sections, both iron and magnesium increase from bottom to top. For the other cross section, no trend can be observed and hence, the trend might be due to heterogeneity.

5.3.2 Caprock

The shale samples have not been studied in detail in the natural analogue study reported in Koenen et al. (2014). For the experimental study, only the one shale sample used in the experiments was investigated. Compared to the sandstone samples, the shale sample is more fine grained, with quartz, mica (biotite, muscovite) and feldspar detrital grains, embedded in a matrix of small quartz and feldspar grains and fine grained clay material. Small dolomites have grown within the clay matrix and are surrounded by patches of magnesium-rich siderite. K-feldspar detrital grains are partially altered to kaolinite (Figure 15). The clay matrix is mainly made up of illite, as previously shown by the XRD analysis (Table 4 and Table 5).
EDX analyses showed that the illite has low to moderate magnesium and iron concentrations (both 0.5 to 1.3 mol%). The average magnesium and iron concentrations of the sample is respectively 1.2 and 1.0 mol% (based on EDX analyses including carbon). Magnesium is present in biotite, muscovite, siderite, dolomite and to a lesser extent in illite. Iron is present in the same minerals, but its concentration in dolomite is low.
After reaction, no significant changes could be observed in the microstructural characteristics. EDX analyses, however, showed some changes within the samples. A geochemical cross section was made by analysing large surface areas (~1.7 mm^2 which is sufficiently large to prevent the effect of heterogeneities) in sequence from bottom to top by EDX. The results are shown in Figure 16. Note that, in contrast to the analyses from the unreacted shales described above, carbon was not included in the quantification since the thin sections prepared from the reacted cubes were impregnated with carbon-containing epoxy.
The cross section shows some variations in elemental concentrations. They could partially be assigned to heterogeneity in e.g. quartz versus feldspar content. On average, the silica content decreases towards the top of the sample, while the calcium, magnesium, iron and aluminium content increase (Figure 16). Several overall measurements were also performed along the top and bottom of the sample (Table 8).
In general, the calcium, magnesium, iron and potassium concentrations are lower in the reacted than the unreacted shale sample (Table 8), which corresponds with the increased concentrations in the formation water. Yet, dolomite and siderite contents did not show a decrease in the XRD analyses, suggesting that these elements have leached from the clay components. The decrease in potassium content corresponds with K-feldspar dissolution.
The leaching of silica from the top corresponds with a decrease in quartz content as measured by XRD and the increased silica concentration in the brine.
XRD results showed the partial conversion of kaolinite to 2:1 clay minerals. The 2:1 clay minerals showed a partial conversion of pure illite to interstratified illite/smectite. For the conversion of kaolinite to illite/smectite requires the availability of cations like potassium, sodium and/or magnesium. Each of these elements showed increased concentrations in the brine. Which type of smectite has formed is unclear.

The ICP-MS analyses of the brine and the leaching water suggested the precipitation of dolomite in the shale cubes as a result of the mixing with fresh water. From the thin sections, this is difficult to observe.

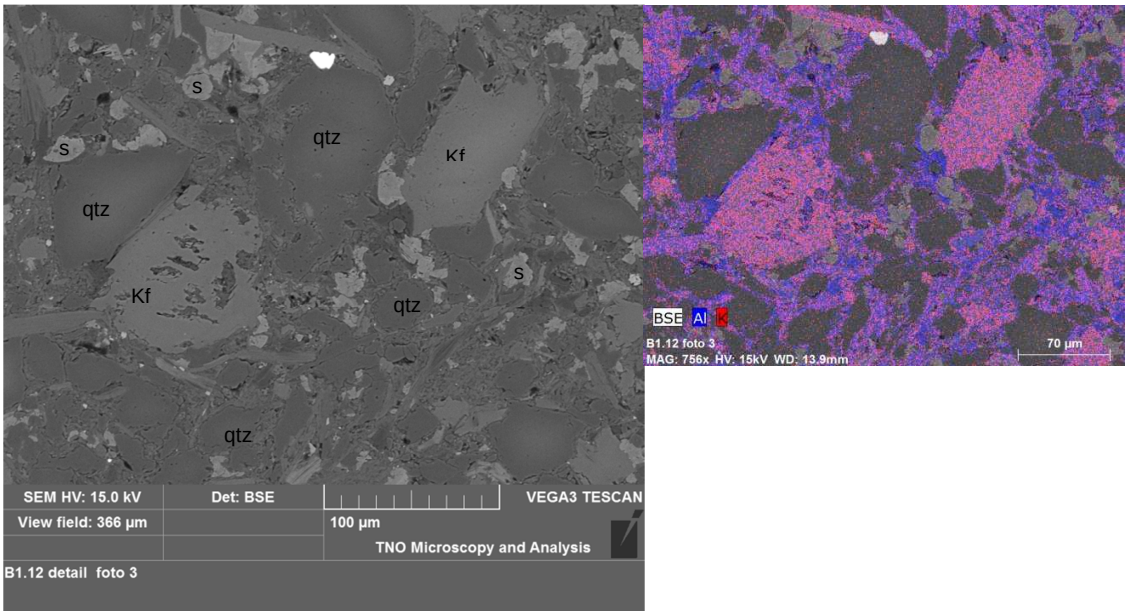

Figure 15. SEM BSE image of unreacted shale sample, showing detrital quartz (qtz) and partially dissolved K-feldspar (Kf) grains, and corresponding element map showing K-feldspar grains, illite (Al- and K-rich clay matrix) and kaolinite (Al-rich clay matrix).

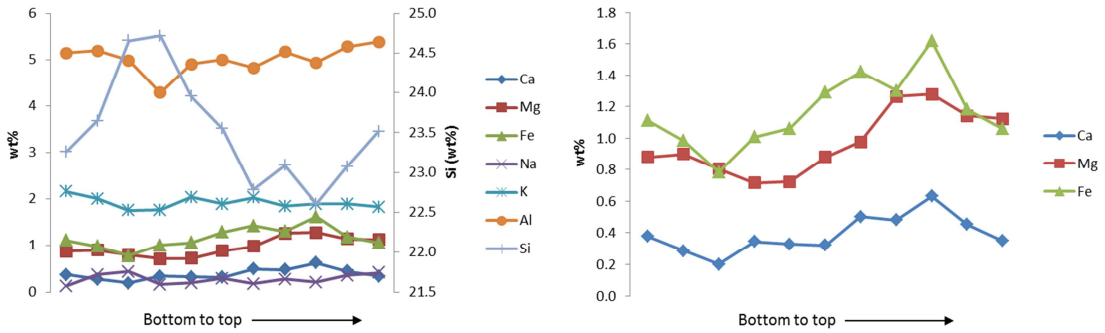

Figure 16. Geochemical cross section from bottom to top. Each measurement represents a surface area of ~1.7 mm^2. Left: all elements shown except for oxygen. Note that silica is shown on the right axis. Right: results for calcium, magnesium and iron only.

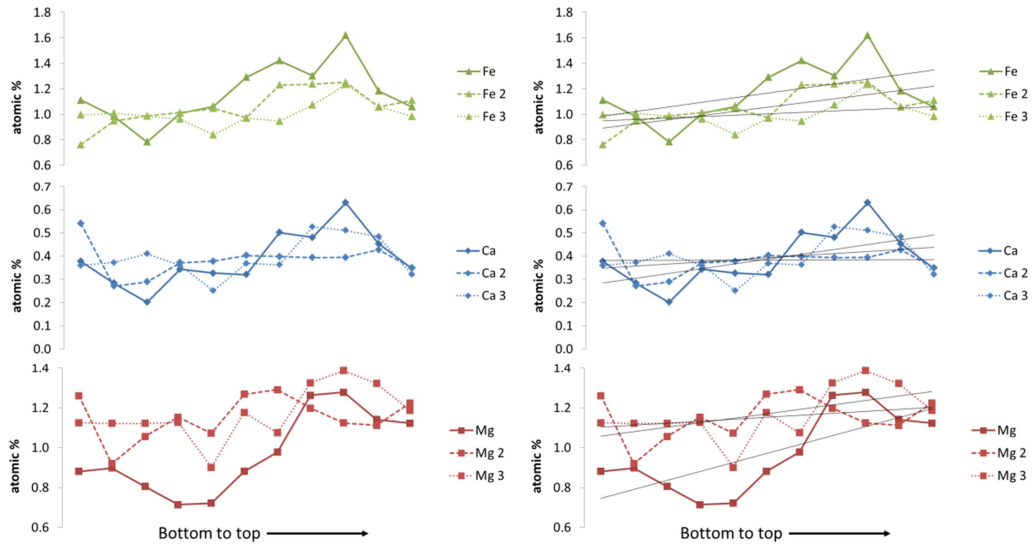

Figure 17. Compilation of three cross sections for iron, calcium and magnesium. The right diagram includes trendlines, which all show enrichment towards the top of the sample.

Table 8. Average compositions of rock samples, normalized without carbon (atomic %).

	O	Na	Mg	Al	Si	K	Ca	Ti	Fe
Average initial shale	66.0	0.4	1.4	5.9	22.3	2.0	0.5	0.2	1.2
Average shale 2	70.1	0.4	1.2	5.2	19.7	1.8	0.4	0.2	1.1
Average shale 3	66.6	0.3	1.0	5.1	23.5	1.9	0.4	0.2	1.1
Top shale 3	66.4	0.3	1.0	5.1	23.2	2.0	0.3	0.1	1.3
Bottom shale 3	66.5	0.4	0.9	4.9	24.1	1.9	0.4	0.2	0.8

6 Geochemical modeling

6.1 Introduction

Geochemical batch modelling was performed using PHREEQC v3 (Parkhurst and Appelo, 2013) to investigate the potential to simulate the CO_2-brine-mineral reactions as observed in the experiments and to calibrate the model according to the results of the natural analogue study. The approach of the geochemical modelling was to investigate which model conditions need to be applied to simulate the mineral reactions observed in the experiments.
Initially, a batch equilibrium model was developed to assess potential secondary minerals and run sensitivity models using various assumptions.
In the modelling, we use the THERMODDEM database developed by BRGM (Blanc et al., 2007). The thermodynamic parameters for ankerite are added to the database (Shell, personal communication):

```
Ankerite
      CaMg0.3Fe0.7(CO3)2 + 2H+ = Ca++ + 0.3Mg++ + 0.7Fe++ + 2HCO3-
      log_k          1.54
      -delta_H       0
      -analytic  -1.8649e+03 -2.9583e-01 1.0468e+05 6.7554e+02 -6.0514e+06
# "analytic" parameters from ToughReact TherAkin8.dat
```

Dissolution and precipitation kinetics are incorporated for silicates using the semi-empirical equation modified from Lasaga (1982) (Palandri and Kharaka, 2004). For each mineral, precipitation constants are assumed to be equal to the dissolution constants.
The reactive surface areas (RSA) of the primary and secondary minerals are calculated using the specific surface area (SSA) of 15.16 and 9.8 m^2/g for clay and non-clay minerals respectively, by the following equation:

RSA = amount of moles * mineral specific molar mass * SSA

At the point of nucleation, when the amount of moles is zero and the SI is positive, a nucleation area of 1e-05 m^2 is used.
Carbonates and sulphate minerals are included in the model as equilibrium phases.

6.2 Input and assumptions

As starting conditions for the reservoir and caprock model, we defined the initial brine composition and the mineralogy. For the brine composition, the artificial brine we developed for the experiments was used:

```
SOLUTION 1 # artificial brine
        temp    110     # °C
        pH      7.0     charge
        pe      -3.5
        redox   pe
        units   mg/l
        Na      35415
        Cl      68408
        Ca      5417
        Mg      1225
        K       1093
        S       147
        density 1
        water   1 # kg
```

For the mineralogy, the results of the XRD analysis were used, complemented by insights from the petrographic analysis.

6.3 Reservoir model

SEM EDX analysis showed that plagioclase is the pure sodium variant albite. The 2:1 Al sheet silicates identified by XRD are subdivided over illite, smectite and muscovite. Illite represents the largest part, as shown by the XRD clay fraction analysis (Table 5) as well as SEM analysis. The illite contains magnesium and iron and hence, illite-IMt-2 is selected ($(Na_{0.044}K_{0.762})(Si_{3.387}Al_{0.613})(Al_{1.427}Fe_{0.376}Mg_{0.241})O_{10}(OH)_2$). In addition, 0.5 wt% of biotite is added (at the expense of quartz). Biotite was not identified by XRD, but shown to be present by SEM analysis. Furthermore, dolomite is subdivided into 'regular' dolomite and iron-rich dolomite (ankerite) based on SEM analysis. The moles per mineral are scaled to a porosity of 13%, 1 liter of formation water and a water saturation of 0.2 (Table 9).

Table 9. Initial (primary) mineralogy used as input for geochemical modelling.

Mineral	wt%	Mol	Remark
Quartz	64.0	961.35	
K-feldspar	9.7	31.45	
Albite	2.1	7.23	Plagioclase identified as albite by SEM EDX analysis
Muscovite	0.5	1.13	Type: Muscovite_ord
Biotite	0.5	1.03	Biotite is added based on SEM analysis; annite
Illite	3.1	7.07	Type: Illite_IMt-2
Smectite	0.2	0.45	Type: SmectiteMX80_des
Kaolinite	2.3	8.04	
Dolomite	1.4	6.85	Dolomite from XRD is subdivided into dolomite and ankerite
Ankerite	1.4	6.12	
Siderite	1.3	10.08	
Anhydrite	13.5	89.25	

The initial solution and mineralogy were equilibrated with a fixed CO_2 partial pressure of 140 bar at a temperature of 110°C, corresponding to the pressure and temperature conditions used in the experiment:

```
GAS_PHASE 1
    -fixed_pressure
    -pressure 140 # bar
    -volume 100
    -temperature 110
    CO2(g) 140
```

The density of the CO_2 at these conditions is approximately 280 kg/m^3, corresponding to approximately 25.5 moles of CO_2 in contact with 1 liter of formation water.

6.3.1 Equilibrium model

In the base case model, only primary minerals are included. Secondary minerals are not allowed to precipitate. This is in accordance to the experimental results (considering that gypsum is probably a reaction product of anhydrite upon pressure release at the end of the experiment). The precipitation of muscovite (a high pressure and temperature metamorphic mineral) is not allowed, since thermodynamic constants of this mineral are inaccurate and usually cause the complete transformation of illite to muscovite.

The results of the base case scenario 1 are shown in Table 10. The model predicts albite, biotite and illite to dissolve. Anhydrite, dolomite, kaolinite and quartz partially dissolve, while ankerite, microcline, siderite and smectite precipitate. These results do not completely correspond to the reactions observed in the experimental study.

In the next model runs, primary and secondary minerals are varied to find a better match with the results of the experimental and petrographic study. The results are shown in Appendix E.
The use of illite-Al ($K_{0.85}Al_{2.85}Si_{3.15}O_{10}(OH)_2$) instead of illite_IMt-2 gives different results which correspond better with the observations from the experiments (Appendix E). This type of illite is more stable and hence, it does not dissolve. The complete dissolution of albite, without smectite precipitation as a sink for Na, results in a very high sodium concentration of > 9 mol/l in the formation water. This is not very realistic. In addition, a lot of silica is released for quartz formation.

In a next model run, the dissolution of albite was limited by allowing a maximum Na concentration in the formation water of ~4 mol/l (Appendix E). As an additional result, the conversion of dolomite, anhydrite and siderite to ankerite is much less. Siderite precipitates in this scenario. The calcium concentration in the formation water is very low (0.002 mol/l) since dolomite and anhydrite dissolution is accompanied by ankerite precipitation. In the experiments, the calcium concentration reaches up to 7 gram/l which is equal to 0.175 mol/l.
Preventing ankerite precipitation, which is not observed in the experiments, results in dolomite precipitation. The calcium concentration in the brine remains low. Preventing the precipitation of ankerite in a model run does not solve this, since anhydrite dissolution only takes place if a sink for calcium is available.

In another run, secondary magnesite was included. Dolomite and (partially) siderite are converted to magnesite and ankerite (Appendix E). The latter two carbonates are more stable than dolomite. The remaining reactions are very similar to those of the previous run.
In the final run, dolomite dissolution was not allowed, since dolomite is always covered by an ankerite rim in the rocks. Now, a small amount of calcite is predicted to precipitate, as well as siderite (Appendix E).

Several runs were performed allowing the precipitation of secondary smectite (various types). However, this was always accompanied by complete illite or albite dissolution and significant K-feldspar precipitation.

Table 10. Base case equilibrium model results. Minerals in red: not corresponding to experimental results.

	Initial (mol)	Final (mol)	Delta (mol)	Experimental results	Brine concentration	
Albite_low	7.23	0.14	-7.09	Dissolution	Al	4.68E-08
Anhydrite	89.25	88.16	-1.09	Dissolution	C	7.53E-01
Ankerite	6.12	8.90	2.78	?	Ca	2.17E-03
Annite	1.03	0	-1.03	?	Cl	2.37E+00
Dolomite	6.85	5.19	-1.66	?	Fe	1.92E-04
Illite_IMt-2	7.07	0.00	-7.07	Precipitation	K	1.22E-01
Kaolinite	8.04	5.10	-2.95	Dissolution	Mg	2.78E-02
Microcline	31.45	37.48	6.03	Possible dissolution	Na	4.23E+00
Muscovite_ord	1.13	1.13	0	?	S	9.81E-01
Quartz,alpha	961.40	956.90	-4.45	Precipitation	Si	1.13E-03
Siderite	10.08	11.39	1.31	Dissolution		
SmectiteMX80_des	0.45	11.67	11.22	Precipitation		

6.3.2 Kinetic model

We chose to select Illite-Al instead of Illite_IMt-2 for the kinetic modelling, with limited albite dissolution, corresponding to the equilibrium model presented in Appendix E, Table 22. The results are shown in Figure 18 and Figure 19 for the mineral reactions and the formation water composition respectively. Dolomite, anhydrite and siderite are quickly, partially converted to ankerite. In addition, smectite, annite kaolinite and (partially) albite and K-feldspar slowly convert to illite and quartz. Siderite initially dissolves, but starts to precipitate after 300-400 years. The iron for siderite originates from the biotite which dissolves very slowly. The porosity changes correspondingly from 13.0% to 13.3%. In total, 4.85 moles of CO_2 are sequestered in ankerite and siderite, corresponding to 19% of the total amount of CO_2 available.
A reference model was run without the presence of CO_2 (Appendix E). A very small amount of dolomite, anhydrite and siderite is converted to ankerite The only major reaction is the transformation of kaolinite and K-feldspar to illite and quartz. Obviously, illite is the more stable clay mineral over kaolinite. Hence, this conversion, which was also predicted in the CO_2 scenario, cannot be linked to the presence of CO_2. Nonetheless, the low pH in the base case scenario accelerates the reaction. In the reference scenario equilibrium is reached after approximately 90,000 years. Albite dissolution is low in this reference scenario and hence significant dissolution did not need to be prevented as in the CO_2 scenario. The formation water composition does not change. The porosity increase is larger than in the base case scenario: 13.4%.

In addition, a kinetic model was run for the scenario in which dolomite is not allowed to dissolve, in correspondence to the results of the petrographic study which shows that dolomite is always covered by ankerite. In this scenario, siderite immediately starts to precipitate, in contrast to the base case in which siderite first dissolves, and then precipitates. Calcite precipitates at the expense of anhydrite, while ankerite precipitation is limited due to a lack of magnesium now that dolomite is not allowed to dissolve. Equilibrium is reached after approximately 70,000 years when 3.80 moles of CO_2 are stored, corresponding to 14.9% of the total amount.

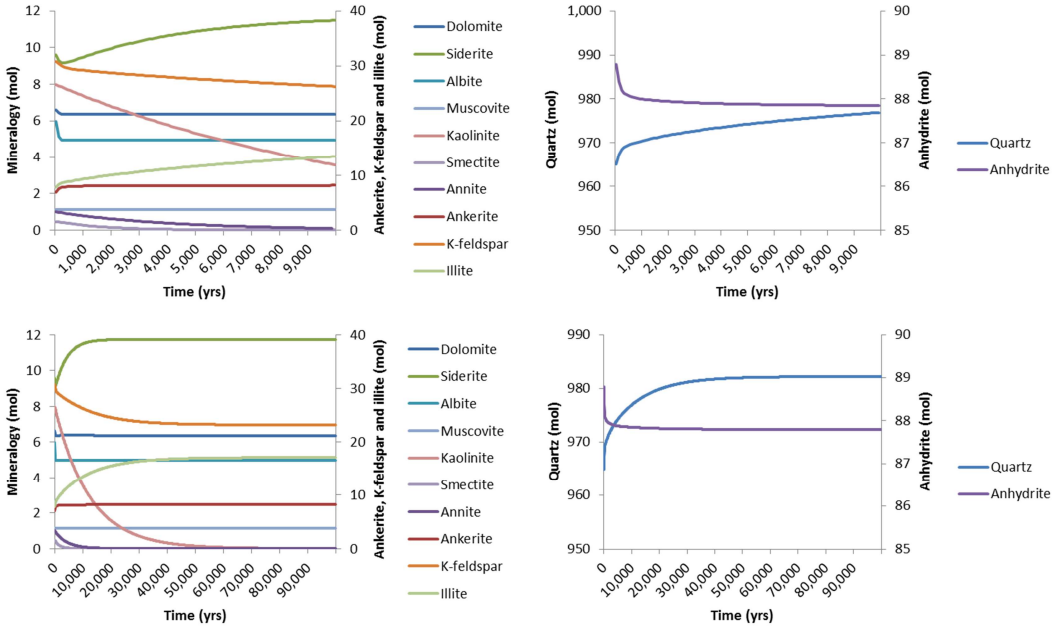

Figure 18. Mineral reactions in time up to 10,000 years (upper) and 100,000 years (lower), predicted by the model with limited albite dissolution. Note that each graph has two y-axes.

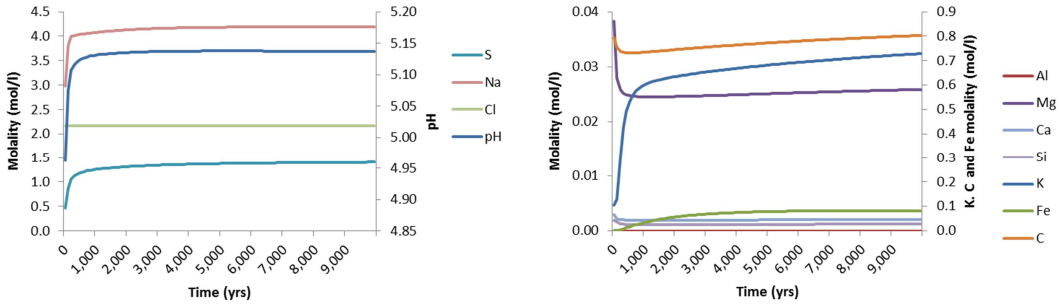

Figure 19. Changes in brine composition with time corresponding to the reaction shown in Figure 18.

6.4 Caprock model

SEM EDX analysis showed that plagioclase is the pure sodium variant albite. The 2:1 Al sheet silicates identified by XRD are subdivided over illite, smectite, muscovite and biotite. Illite represents the largest part, as shown by the XRD clay fraction analysis (Table 5) as well as SEM analysis. The illite contains magnesium and iron and hence, illite-IMt-2 is selected ($(Na_{0.044}K_{0.762})(Si_{3.387}Al_{0.613})(Al_{1.427}Fe_{0.376}Mg_{0.241})O_{10}(OH)_2$). The moles per mineral are scaled to a porosity of 5%, 1 liter of formation water and a water saturation of 1 (Table 11). Like for the sandstone samples, the initial solution and mineralogy were equilibrated with a fixed CO_2 partial pressure of 140 bar at a temperature of 110°C in the thermodynamic batch model, corresponding to the pressure and temperature conditions used in the experiment.

Table 11. Initial (primary) mineralogy used as input for geochemical modelling.

Mineral	wt%	Mol	Remark
Quartz	43.7	374.52	
K-feldspar	8.8	16.28	
Albite	1.7	3.34	Plagioclase identified as albite by SEM EDX analysis
Muscovite	0.8	1.03	Type: Muscovite_ord
Biotite	0.9	1.05	Biotite is added based on SEM analysis; annite
Illite	3.1	7.07	Type: Illite-Al
Smectite	8.5	10.97	Type: SmectiteMX80_des
Kaolinite	4.1	8.18	
Dolomite	1.4	3.95	
Siderite	3.8	16.82	
Calcite	0.6	3.09	

6.4.1 Equilibrium model

In the first equilibrium model, only primary minerals are included. No additional secondary minerals are not allowed to precipitate, which is in accordance to the experimental results. A small amount of dolomite is replaced by ankerite to account for possible zonation of dolomite (Fe-rich dolomite rims). These rims were observed in the sandstone rocks but it is unclear whether they are present in the clay-rich rocks. The precipitation of muscovite and biotite (a high pressure and temperature metamorphic mineral) is not allowed. The results show reasonable conformance with the experimental results, except for the dissolution of albite and smectite, and the precipitation of quartz (Table 12).
In the second model run primary ankerite was excluded. No additional secondary minerals are not allowed to precipitate. The results now show the precipitation of dolomite instead of ankerite, and much more siderite precipitated. Also, albite precipitated in this model (Table 13), which corresponds to the experimental results.
In a third model run, primary ankerite is excluded, but secondary carbonates are allowed to precipitate (ankerite and magnesite). The results are shown in Table 14. Quartz precipitation and siderite and smectite dissolution are not according to the experimental results. In addition, some carbonate interaction occurs. Dolomite and calcite are not stable together, and react with siderite to form ankerite. The dissolution of smectite is enhanced to provide additional cations for the carbonate transformation.

Table 12. Base case equilibrium model results. Minerals in red: not corresponding to experimental results.

	Initial (mol)	Final (mol)	Delta (mol)	Experimental results	Brine concentration	
Albite_low	3.34	2.20	-1.14	Precipitation	Al	2.71E-08
Ankerite	0.50	4.86	4.36		C	2.73E+00
Annite	1.05	0.00	-1.05	?	Ca	2.61E-04
Calcite	3.09	0.00	-3.09	Dissolution?	Cl	2.13E+00
Dolomite	3.95	2.86	-1.09	?	Fe	1.13E+00
Illite-Al	33.19	42.64	9.45	Precipitation?	K	8.94E-02
Kaolinite	8.18	0.00	-8.18	Dissolution	Mg	7.29E-05
Microcline	16.28	9.26	-7.02	Dissolution	Na	3.34E+00
Muscovite_ord	1.03	1.03	0.00	?	S	5.05E-03
Quartz,alpha	374.50	391.20	16.69	Dissolution	Si	1.12E-03
Siderite	16.82	16.95	0.13	Precipitation?		
SmectiteMX80_des	10.97	10.29	-0.68	Precipitation		

Table 13. Equilibrium model results excluding primary ankerite. Minerals in red: not corresponding to experimental results.

	Initial (mol)	Final (mol)	Delta (mol)	Experimental results	Brine concentration	
Albite_low	3.34	4.55	1.21	Precipitation	Al	2.71E-08
Annite	1.05	0.00	-1.05	?	C	2.73E+00
Calcite	3.09	1.64	-1.45	Dissolution?	Ca	2.61E-04
Dolomite	3.95	5.65	1.70	?	Cl	2.13E+00
Illite-Al	33.19	47.85	14.66	Precipitation?	Fe	1.13E+00
Kaolinite	8.18	0.00	-8.18	Dissolution	K	8.94E-02
Microcline	16.28	4.99	-11.29	Dissolution	Mg	7.29E-05
Muscovite_ord	1.03	1.03	0.00	?	Na	3.34E+00
Quartz,alpha	374.50	404.00	29.43	Dissolution	S	5.05E-03
Siderite	16.82	20.24	3.42	Precipitation?	Si	1.12E-03
SmectiteMX80_des	10.97	3.81	-7.16	Precipitation		

Table 14. Equilibrium model results excluding primary ankerite, including secondary carbonate minerals. Minerals in red: not corresponding to experimental results.

	Initial (mol)	Final (mol)	Delta (mol)	Experimental results	Brine concentration	
Albite_low	3.34	5.98	2.64	Precipitation	Al	2.60E-08
Ankerite	0.00	7.32	7.32		C	3.29E+00
Annite	1.05	0.00	-1.05	?	Ca	8.10E-05
Calcite	3.09	0.00	-3.09	Dissolution?	Cl	2.11E+00
Dolomite	3.95	0.00	-3.95	?	Fe	1.71E+00
Illite-Al	33.19	50.89	17.70	Precipitation?	K	9.43E-02
Kaolinite	8.18	0.00	-8.18	Dissolution	Mg	4.59E-05
Magnesite(Natur)	0.00	4.32	4.32		Na	3.50E+00
Microcline	16.28	2.49	-13.79	Dissolution	S	5.00E-03
Muscovite_ord	1.03	1.03	0.00	?	Si	1.09E-03
Quartz,alpha	374.50	411.30	36.81	Dissolution		
Siderite	16.82	15.26	-1.56	Precipitation?		
SmectiteMX80_des	10.97	0.00	-10.97	Precipitation		

6.4.2 Kinetic model

The second equilibrium model was selected for the kinetic modelling (according to Table 13) was run with kinetics included. The model results (Figure 20) show initial albite dissolution, but precipitation starts after a few hundreds of years. On the long-term, kaolinite, microcline, smectite, annite and calcite (partially) dissolve to form siderite, dolomite, illite and quartz. The iron for siderite precipitation is provided by smectite and annite. Calcium and magnesium for dolomite is provided by calcite and smectite. The porosity decreases slightly from 5.00 to 4.82% as a result of these reactions, as calculated using molar volumes.

A reference model without high CO_2 partial pressure was run to identify any reactions predicted as a result of 'ordinary' diagenetic processes. The results (Appendix F, Figure 27) show the conversion of kaolinite and partially microcline to illite and quartz. Hence, this reaction, which was also predicted in the CO_2 model, could not be assigned to the presence of CO_2.Therefore, in a next model run, kaolinite dissolution was prevented while applying the high CO_2 partial pressure. Similar reactions occur as for the first kinetic model, except that kaolinite does not react with microcline (Appendix F, Figure 28). Instead, a more limited amount of microcline is dissolved and the amount of illite and quartz precipitation is lower.

Biotite is the only mineral that is completely dissolved. The porosity change as a result of these reactions, calculated using molar volumes, is negligible (from 5.00% to 4.97%).

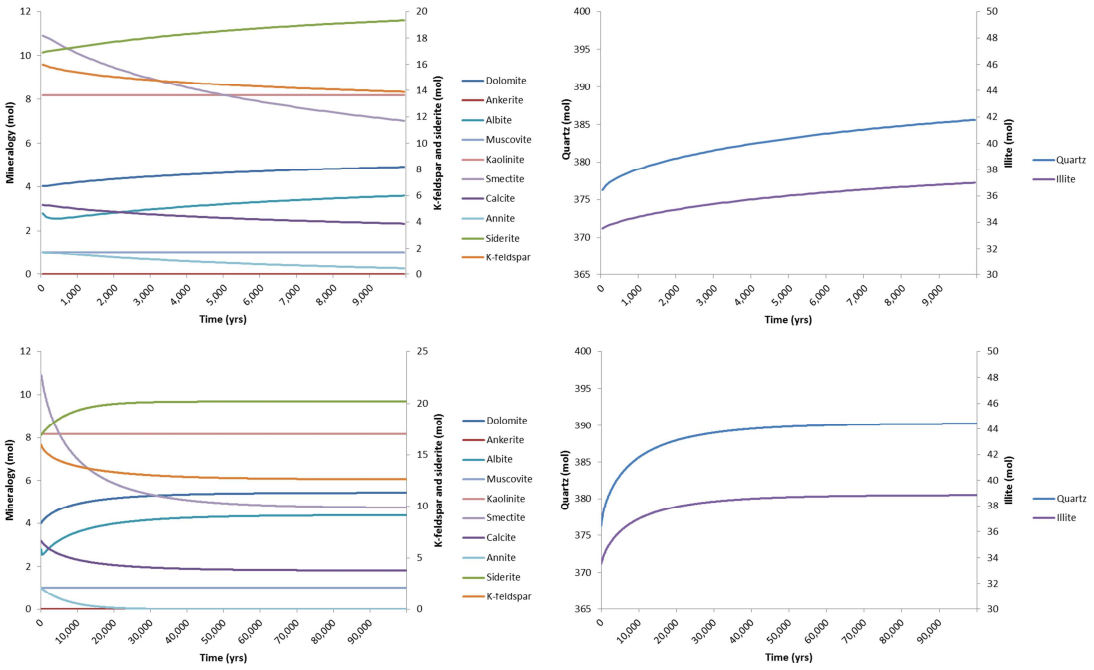

Figure 20. Mineral reactions in time up to 10,000 years (upper) and 300,000 years (lower) for the CO_2 model without primary ankerite. Note that each graph has two y-axes.

7 Implications for CO_2 storage

Laboratory experiments were performed using Barendrecht-Ziedewij sandstone material to assess the reactivity of the minerals at high CO_2 partial pressures. The results were subsequently supported by geochemical modelling, whereas the geochemical model, on the other hand, is validated using the results from the laboratory experiments.

7.1 CO_2 sequestration in the reservoir

7.1.1 Experiments and model validation

The XRD and ICP-MS results of the reacted sandstone material after 4, 8 and 12 months suggested the following overall reaction:

K-feldspar + kaolinite + siderite + dolomite (+ anhydrite) → quartz + illite + smectite

Potentially some anhydrite dissolved, but part of the anhydrite dissolution seems to have occurred during washing of the powder material. It is unclear what caused the red coloration of the upper part of the rock cubes. Geochemical cross sections indicated potential iron and magnesium increase towards the top of the cube, but this might be due to heterogeneity. Even though the sandstone material was powdered to increase the reactive surface area of the minerals, experimental studies can only assess short time periods. Geochemical modelling is required to extrapolate experimental results to longer time scales.

Geochemical modelling results showed that the predicted geochemical reactions are affected by the selection of input parameters as well as selection of secondary minerals. The type of illite selected as primary mineral can dominate the majority of the reactions. The Illite_IMt-2 was predicted to be unstable and its dissolution resulted in a release of cations for carbonate formation. Since our experimental results suggested illite precipitation instead of dissolution the selection of the stable Illite-Al fits better with the experiments. The dissolution of albite had to be limited artificially in order to keep the sodium concentration in the brine at realistic values. It is unclear why the dissolution of albite continued up to such high sodium values.
The kinetic model showed the complete dissolution of annite, smectite and kaolinite and the partial dissolution of K-feldspar to form illite and quartz. Except for the dissolution of smectite, this corresponds with the experimental results. In addition, some anhydrite dissolved on the short term for the precipitation of additional ankerite.

Smectite clay is generally unstable at the depths considered for CO_2 storage. Smectite can form as an alteration product at the earth surface or at shallow burial depths, but it is known to alter to illite or chlorite by progressive replacement with increasing burial depth (Worden and Burley, 2003). In several experimental studies, the formation of smectite has been observed. Hebner et al., (1986) observed the formation of smectite as a result of steam injection for enhanced oil recovery purposes. The amount of smectite which precipitated in their experiments was directly proportional to the amount of magnesium and calcite in the formation water (and hence the amount of dolomite present) and the amount of kaolinite. Our experiments showed the dissolution of dolomite and kaolinite, and hence our results correspond to their reaction induced by steam injection. A possible explanation is that a sudden perturbation of the geological system, by e.g. steam injection or CO_2 influx, can result in the temporary formation of meta-stable smectite. A geochemical model based on thermodynamic constants will not predict meta-stable mineral formation, and for long-term effects, the dissolution of smectite is more realistic. Credoz et al.

(2011) report on an experimental study showing the enhanced illitization of interstratified illite/smectite in the presence of high CO_2 partial pressures by the following reaction: I/S + K (from K-feldspar) → illite + SiO_2, which corresponds to our long-term model prediction.

Siderite and dolomite are predicted by the model to partially dissolve in the initial phase, corresponding to the experimental results. However, siderite starts precipitating on the longer term. Initial dissolution of carbonates is a well-known process at high CO_2 partial pressures for pH buffering. At the longer term, silicates take over the buffering process, thereby releasing cations for the subsequent (re-)precipitation of carbonates. Hence, the dissolution of siderite in the experiments is consistent with the kinetic model. On the long-term, siderite is able to sequester part of the CO_2. After equilibrium is reached, predicted to occur after approximately 90,000 years, 19% of the CO_2 is simulated to have been sequestered in ankerite and siderite.

The model predicted the transformation of kaolinite and K-feldspar to illite and quartz regardless of the presence of CO_2, suggesting that illite is the more stable clay mineral over kaolinite. Yet, kaolinite is abundant in the rock samples of the Barendrecht-Ziedewij sandstones and no signs of illitization were observed.

SEM analyses showed that dolomite is generally enclosed by Fe-rich dolomite (ankerite) in the rock samples. This basically means that the reactive surface area of dolomite is zero. Powdering of the rock samples for the experiments increased the reactive surface area and hence, allowed dolomite to dissolve. Taking into account the negligible reactive surface area of dolomite in the geochemical model gave slightly different results. In this scenario, only 15% of the CO_2 is sequestered, due to limited ankerite precipitation.

7.1.2 Comparison to Werkendam analogue

The Barendrecht-Ziedewij field was selected as a CO_2-free stratigraphic analogue for the Werkendam CO_2 field. Based on petrographic and mineralogical analyses, which are described in detail in Koenen et al. (2014), the following diagenetic mineral reactions observed in the Werkendam sandstones are assigned to the presence of CO_2:

K-feldspar + anhydrite + Mg^{2+} + Fe^{2+} → Mg-rich siderite + quartz + barite + Ca^{2+} + K^{+} + Al^{2+}

A possible source of iron for the siderite is hematite. Any remnants of this mineral were not observed by scanning electron microscopy, but hematite dissolution and iron oxidation due to hydrocarbon charging is a common process, causing the bleaching of red sediments (Gaupp and Okkerman, 2011). The liberated iron could subsequently be used in the formation of siderite after CO_2 influx. The source of magnesium is currently unknown. In addition, we did not observe any sink for calcium, potassium and aluminium in the samples analysed. Based on the lack of several sources and sinks, mass transfer to and away from the sandstone layers seems likely. The Werkendam reservoir contains many clay rich intervals within the Röt Fringe Sandstone Member, and mass transfer between the clay-rich interval and the sandstone layers might have occurred.

The experimental results, supported by geochemical modelling, suggested the following reactions to occur if CO_2 would be stored in the Barendrecht-Ziedewij reservoir:

smectite + biotite + anhydrite + albite (+ K-feldspar + kaolinite) → siderite + ankerite + illite + quartz

Part of the reaction is similar to the reactions observed for Werkendam. In the Barendrecht-Ziedewij samples, biotite and smectite provide the iron for siderite, instead of hematite. Biotite is not present as a primary mineral in Werkendam. The dissolution of anhydrite and K-feldspar and

the precipitation of siderite and quartz are similar. The amount of siderite which sequesters CO_2 is large for Werkendam, and precipitation of ankerite, as well as illite was not observed. The ankerite and illite are the sinks for calcium, potassium and aluminium for Barendrecht-Ziedewij, which are lacking in the Werkendam samples. Hence, ankerite and illite precipitation might have occurred in the clay-rich intervals within the Röt Fringe Sandstone Member.

Barite was not included in the geochemical model. Barium is a common impurity in K-feldspar. Barite precipitation in Werkendam sandstones is thought to be the result of barium release upon K-feldspar dissolution and subsequent reaction with sulfate from anhydrite dissolution.

7.2 Caprock sealing integrity

7.2.1 Geochemical reactions

A shale caprock is a clay-rich material, saturated with water and having a low permeability and high capillary entry pressure (Bildstein et al., 2010). The sealing integrity of a caprock needs to be sustained for long time scales. Since reactivity of rocks is highly site specific, depending on the mineralogy, brine composition and pressure and temperature conditions, geochemical assessment of selected sites for potential CO_2 storage is required.

In this study, geochemical batch experiments were performed using Barendrecht-Ziedewij clay-rich siliciclastic material to investigate the potential contribution of such experimental studies in site specific, geochemical evaluations for the purpose of caprock integrity assessment.
The XRD and ICP-MS results of the reacted powder material after 4, 8 and 12 months show that some reactions have occurred. Yet, the changes in mineralogy with time are minor, and in addition they do not show progressive trends with time for every mineral (in XRD analyses) or elemental concentration in the brine (in ICP-MS analyses). Overall, the following reaction is suggested:

K-feldspar + quartz + kaolinite (+ calcite + dolomite) + CO_2 → illite + smectite + albite

This reaction would require additional sodium from the brine for albite precipitation. Dolomite could provide calcium and/or magnesium for smectite. Calcite dissolution was potentially observed from XRD analyses, while dolomite dissolution was interpreted from ICP-MS results but is not consistent with XRD results.
This reaction is very similar to the results from Bateman et al. (2014) who performed batch experiments on Utsira caprock or 5 years. Even though the authors concluded not to have any definitive evidence for mineral changes other than calcite dissolution, the XRD results before and after the experiment suggest the following reaction:

K-feldspar + kaolinite + calcite + chlorite + CO_2 → mica (illite) + quartz + albite

The reacted rock cubes in this study did not give any additional results. Like for the reservoir rock cube, geochemical cross sections indicated potential iron and magnesium and potentially calcium increase towards the top of the cube, possibly suggesting additional carbonate precipitation in the upper part of the cube. However, this is not consistent with XRD and ICP-MS analyses which showed carbonate dissolution. No significant changes could be observed between the rock before and after the experiment, due to the heterogeneity of the rock samples as well as low reactive surface area of the minerals. Hence, powdering of caprock material is crucial if experimental studies are performed for such (relatively) short periods of time.

Geochemical modelling showed that CO_2 is sequestered in siderite and dolomite. Biotite, smectite and calcite provide the required cations. Albite is formed on the long term due to liberation of sodium from smectite dissolution. In addition, the transformation of K-feldspar and kaolinite to illite and quartz is predicted. However, this reactions was also predicted in the reference model without applying a high CO_2 partial pressure.
When excluding the dissolution of kaolinite in the model, K-feldspar is partially illitized, thereby releasing silica for quartz precipitation. feldspar is known to be unstable at low pH conditions. Yet, only part of the feldspar is dissolved, once equilibrium is reached. The overall reaction from the geochemical modelling can be summarized as follows:

K-feldspar (± kaolinite) + smectite + biotite + calcite + CO_2 → siderite + dolomite + illite + albite + quartz

Like for the reservoir model, the reaction of kaolinite with K-feldspar to illite and quartz is also predicted in the reference scenario. Since kaolinite is currently still present in the rock samples, this reaction did not occur during the history of the rocks. The experimental study, on the other hand, did suggest the transformation of kaolinite to illite. Possibly, nucleation of illite is stimulated by powdering of the rock sample.
The reaction from geochemical modelling does not completely correspond to the reactions deduced from the experiments. Biotite was not identified in XRD of the rock samples and hence it is not known whether biotite dissolution occurred. However, biotite alteration to siderite is a common diagenetic process and was observed in the sandstone rocks of the Barendrecht-Ziedewij field (section 5.3.1). In the experiment, smectite formation was observed. Like for the reservoir experiment, a sudden perturbation of the geological system, by e.g. CO_2 influx, might result in the temporary formation of meta-stable smectite. On the long-term, the smectite would not be stable and hence, the model prediction of smectite to illite seems more straightforward. The dissolution of quartz during the experiments, as identified by XRD is difficult to explain. Generally, most reactions involve the *release* of silica and hence cause *precipitation* of quartz (e.g. K-feldspar/kaolinite illitization) (Jonas and McBride, 1977).

To summarize, the reactions observed from the experimental study do not seem very reliable and they do not correspond well with the geochemical model results. Partially, this can be explained by short-term versus long-term effects and the potential formation of metastable minerals during the experiments. In addition, heterogeneities in the powder material might have resulted in trends which are not progressive with time, even though the powder material was mixed prior to filling of the holders at the start of the experiment.

7.2.2 Transport properties

The reactions predicted by geochemical modelling resulted in slight porosity decreases, based on molar volume changes. The geochemical models represent kinetic batch models, assuming full water saturation, with the brine in equilibration with the CO_2 partial pressure as applied for the reservoir (140 bar), corresponding to the experimental conditions from this study.
Assuming that the injected CO_2 pressure will not exceed the CO_2 capillary entry pressure and no significant fractures exist, the only migration process of CO_2 into a caprock is by slow, upward diffusion of dissolved CO_2. The mineralogy of the caprock can subsequently interact with the carbonized brine, thereby affecting the sealing properties of the caprock. The process of upward diffusion was already reported by Tambach et al. (2012). The model results showed migration of CO_2 up to maximally 16 meter into the caprock after 10,000 years for a clay-rich caprock (Tambach et al. 2012). Diffusion models generally show a slight porosity *in*crease or *de*crease of the caprock, depending on the primary mineralogy as well as the selection of secondary minerals, but the alteration remains limited to the first few meters at the contact with the reservoir rock (Gaus et al., 2005, Bildstein et al., 2010 and Tambach et al., 2011).

The sealing potential of shale caprocks depends on the high specific surface area of clays since they increase the capillary entry pressure of the rocks (Espinoza and Santamarina, 2012). The reaction of kaolinite and especially K-feldspar to illite could result in a permeability decrease. Due to its general fibrous habit, illite might decrease the permeability, even though it hardly affects porosity, (Morad et al., 2010, Credoz et al., 2011) and increase the specific surface (Espinoza and Santamarina, 2012). This would improve the sealing integrity of the caprock by slowing down the upward diffusion of the CO_2.

7.3 Implications for geochemical modelling

The occurrence and process of illitization of kaolinite and/or K-feldspar is still not well understood. As a result, the stability of these minerals in geochemical databases is not well implemented and careful interpretation of geochemical predictions is required. It is possible, that the illitization of kaolinite and K-feldspar is enhanced or stimulated by the presence of high CO_2 partial pressures. The experimental results suggested that this reaction had started. However, kaolinite is generally assumed to be the clay mineral stable at lower pH conditions than illite. Hence, overall we cannot not say with confidence that this reaction would occur if CO_2 would be stored in this reservoir. In the absence of this reaction, the dissolution of albite, smectite and biotite, as predicted in the model, can account for the formation of illite and quartz.

8 Concluding remarks

Short-term experimental studies and long-term geochemical modeling are complementary techniques for the geochemical evaluation of CO_2 behaviour in a reservoir and on caprock integrity. The results from this study show that experimental studies can help in the assessment of the gas-water-rock interactions. Powdering of rock material is required to increase the reactive surface area and enhance reaction kinetics. However, powdering of the rocks destroys the rock textures which are crucial in the geochemical interactions. Careful interpretation of the experimental results is necessary and need support from petrographic analyses and geochemical modelling. Geochemical modelling, on the other hand, also requires careful interpretation since they are based on thermodynamic databases which are dealing with great uncertainties and oversimplified conditions. In addition, model results are sensitive to the selected input parameters and a thorough sensitivity analysis should be part of every geochemical assessment for a site evaluation.

9 References

Bateman K., Rochelle C.A., Purser G., Kepm S.J. and Wagner D. (2013). Geochemical interactions between CO_2 and minerals within the Utsira caprock: A 5-year experimental study. Energy Procedia 37, 5307-5314.

Bildstein O., Kervévan C., Lagneau V., Delaplace P., Crédoz A., Audigane P., Perfetti E., Jacquemet N. and Jullien M. (2010). Integrative modeling of caprock integrity in the context of CO_2 storage: evolution of transport and geochemical properties and impact on performance and saety assessment. Oil & Gas Science and Technology – Rev. IFP 65 (3), 485-502.

Blanc, P., Lassin, A., Piantone, P., 2007. THERMODDEM A DATABASE DEVOTED TO WASTE MINERALS. BRGM, Orléans, France. http://thermoddem.brgm.fr.

Credoz A., Bildstein O., Jullien M., Raynal J., Trotignon L. and Pokrovsky O. (2011). Mixed-layer illite-smectite reactivity in acidified solutions: Implications for clayey caprock stability in CO_2 geological storage. Applied Clay Science 53, 402-408.

Gaus I., Azaroual M. and Czernichowski-Lauriol I. (2005). Reactive transport modelling of the impact of CO_2 injection on the clayey cap rock at Sleipner (North Sea). Chemical Geology 217, 319-337.

De Vos W. and Tarvainen T. (2006). Geochemical Atlas of Europe – Part 2: Interpretation of geochemical maps, additional tables, figures, maps, and related publications. Geological Survey of Finland, Otamedia Oy, Espoo. ISBN 951-690-960-4, 692 p.

Espinoza E.N. and Santamarina J.C. (2012). Clay interaction with liquid and supercritical CO_2: The relevance of electrical and capillary forces. International Journal of Greenhouse Gas Control 10, 351-362.

Gaupp R. and Okkerman J.A. (2011). Diagenesis and reservoir quality of Rotliegend sandstones in the northern Netherlands – a review. In: The Permian Rotliegend of the Netherlands. SEPM Special Publication No. 98. ISBN 978-1-56576-300-5, 193-226.

Heath J.E., Dewers, T.A., McPherson B.J.O.L., Nemer M.B. and Kotula P.G. (2012. Pore-lining phases and capillary breakthrough pressure of mudstone caprocks: Sealing efficiency of geologic CO_2 storage sites. International Journal of Greenhouse Gas Control 11, 204-220.

Hebner B.A., Bird G.W. and Longstaffe F.J. (1986). Fluid/pore-mineral transformations during simulated steam injection: implications for reduced permeability damage. The Journal of Canadian Petroleum Technology, p 68 – 73.

IPCC (2005). IPCC special report on carbon dioxide capture and storage. Prepared by Working Group III of the Intergovernmental Panel on Climate Change. Cambridge University Press, Cambridge, United Kingdom and New York, NY, USA.

Jacobson R.L. and Usdowski H.E. (1976). Partitioning of strontium between calcite, dolomite and liquids: An experimental study under higher temperature diagenetic conditions, and a model for

the prediction of mineral pairs for geothermometry. Contributions to Mineralogy and Petrology 59, 171-185.

Jonas E.C. and McBride E.F. (1977). Diagenesis of sandstone and shale: application to exploration for hydrocarbons. Department of geological sciences, The university of Texas at Austin, Austin, Texas 78712, 169 p.

Koenen M., Wasch L., Waldmann S. and Nelskamp S. (2014). Mineralogical and microstructural characteristics of the Werkendam field related to long term CO_2 induced reactions: analytical/mineralogical data on reservoir evolution. CATO-2 Deliverable WP3.3 D28.

Kramm U. and Bless M.J.M. (1986). Sr isotopic analysis of anhydrites and pseudomorphs of calcite after anhydrite from visean rocks of Heugem (South Limburg, Netherlands) and St-Ghislain (SW Belgium) – short note. Annales de la Société géologique de Belgique 109, 603-607.

Lanson B., Beaufort D., Berger G., Baradat J. and Lacharpagne J-C. (1996). Illitization of diagenetic kaolinite-to-dickite conversion series : late-stage diagenesis of the lower Permian Rotliegend Sandstone reservoir, offshore ot the Netherlans. Journal of Sedimentary Research ; 66 (3), 501-518.

Lanson B., Beaufort D., Berger G. Bauer A., Cassagnabère A. and Meunier A. (2002). Authigenic kaolin and illitic minerals during burial diagenesis of sandstones : a review. Clay minerals; 37, 1-22.

Morad S., Al-Ramadan K., Ketzer J.M. and De Ros L.F. (2010). The impact of diagenesis on the heterogeneity of sandstone reservoirs: A review of the role of depositional facies and sequence stratigraphy. AAPG Bulletin 94)8), 1267-1309.

Parkhurst D.L. and Appelo C.A.J. (2013). Description of input and examples for PHREEQC Version 3 – A computer program for speciation, batch-reaction, one-dimensional transport, and inverse geochemical calculations. U.S. Geological Survey. Techniques and Methods, book 6, chapter A43, 497 p., available only at http://pubs.usgs.gov/tm/06/a43.

Tambach T.J., Koenen M., Wasch L.J. and van Bergen F. (submitted for International Journal of Greenhouse Gas Control). Geochemical evaluation of CO_2 injection and containment in a depleted gas field.

Tambach T., van Bergen F., Gutierrez-Neri M., Hofstee C., Koenen M., Kooi H., Loeve D., Maas J., Plug W-J., Ranganathan P., Roels S., van der Meer B., Wasch L. and Zitha P. (2012). Models describing near-well clogging and mineralization to support feasibility and long-term integrity. CATO-2 Deliverable WP3.02-D13.

Wollenweber J., Alles S., Busch A., Krooss B.M., Stanjek H. and Littke R. (2010). Experimental investigation of the CO_2 sealing efficiency of caprocks. International Journal of Greenhouse Gas Control 4, 231-241.

Worden R.H. and Morad S. (2003). Clay minerals in sandstones: controls on formation, distribution and evolution. In: Clay mineral cements in sandstones, edited by R. Worden and S. Morad. ISBN 1-40510-587-9.

Worden R.H. and Burley S.D. (2003) Sandstone diagenesis: the evolution of sand to stone. In: Sandstone diagenesis – Recent and Ancient 4, 3-44.

Zhou D. and Stenby E.H. (1993). Interpretation of capillary pressure curves using invasion percolation theory. Transport in Porous Media 11, 17-31.

Appendix A

Table 15. Brine sample concentrations in mg/l for the reservoir experiments. values in µg/l. Green: high Al value suggesting clay entrainment.*

		Li*	Na	Mg	Al	Si	S	Cl	K	Ca	V	Mn*	Fe	Co*	Ni*	Cu*	Zn*	Sr*	Ba*	Pb*
4 months	filtered brine	1650.9	26945.5	1040.6	1.3	176.9	-	51360.9	1282.0	4597.1	-	3351.6	100.3	0.0	19003.1	546.6	80948.0	18290.4	2132.8	208.6
	Clear brine	1789.1	33266.4	1142.9	1.9	191.6	-	58396.3	1436.5	5026.0	-	3661.5	90.3	0.0	23404.3	607.6	92897.2	20070.2	2376.4	174.6
	turbid brine	1747.3	29091.3	1137.8	8.6	221.1	-	56751.8	1399.4	5006.8	-	3773.0	153.7	0.0	21182.7	908.2	96059.6	20178.2	2422.6	484.5
	washing water	279.4	4328.8	175.4	0.1	24.0	-	8813.5	213.0	897.5	-	659.5	10.1	0.0	2765.9	76.8	10964.4	4282.1	182.6	5.4
8 months	filtered brine	3420.8	37490.0	1640.9	-	168.4	552.3	80848.0	1922.3	6357.0	-	-	-	190.9	1329.7	2698.9	7255.3	46183.3	2566.7	416.2
	Clear brine	3499.0	43672.3	1929.9	-	195.6	-	83856.8	2226.7	6980.3	-	-	-	220.9	1559.3	3199.4	8826.3	53291.7	3388.6	529.2
	turbid brine	3967.3	47268.6	2052.9	-	236.4	-	91227.8	2425.0	7846.2	-	-	55.8	241.3	1677.7	3438.0	10257.0	56661.4	3794.0	1028.2
	washing water	839.1	10310.0	445.5	-	45.9	340.8	22900.0	496.7	1974.0	2.2	306.3	3.6	51.4	361.1	662.6	1283.0	14520.0	419.6	70.5
	leaching water	44.3	525.6	20.4	-	-	85.8	1018.0	33.5	158.2	-	-	-	2.7	19.8	9.5	49.3	1376.0	27.2	-
12 months	filtered brine	2784.7	38246.1	1481.5	-	222.1	587.3	77893.4	1761.4	6478.7	-	2293.5	38.5	205.8	784.1	1490.2	5002.7	36656.0	2951.2	491.6
	Clear brine	3544.7	47117.9	1834.8	-	298.3	795.5	106058.7	2197.8	7932.7	-	2613.4	45.3	269.9	1068.2	2036.4	6710.2	44939.1	3871.3	786.7
	turbid brine	2802.3	40152.8	1551.1	-	241.4	-	85151.1	1853.3	6566.0	-	2683.0	61.0	232.3	1301.2	1693.8	6081.4	38089.3	3262.9	915.8
	washing water	693.3	10440.0	403.7	-	53.2	343.6	23100.0	440.4	2040.0	2.4	605.4	7.3	53.3	183.2	410.1	886.8	11730.0	450.8	54.4
	leaching water	25.4	336.9	11.5	-	-	198.7	763.8	20.8	276.0	-	43.3	-	2.6	7.3	-	-	2612.0	18.6	-

*Table 16. Brine sample concentrations in mg/l for the caprock experiments. *values in µg/l. Green: high Al value suggesting clay entrainment.*

		Li*	Na	Mg	Al	Si	S	Cl	K	Ca	V	Mn*	Fe	Co*	Ni*	Cu*	Zn*	Sr*	Ba*	Pb*
4 months	filtered brine	-	-	-	-	-	-	-	-	-	-	-	-	-	-	-	-	-	-	-
	Clear brine	7688.1	41909.7	1789.5	1.6	104.2	-	84035.0	1749.3	6679.7	-	2110.9	25.8	0.0	1282.8	2184.4	11544.4	26714.8	2567.6	5649.7
	turbid brine	8085.0	43198.4	1916.9	138.3	382.9	-	84270.2	1844.4	6934.5	-	4902.0	270.9	0.0	1895.3	2468.6	17708.6	28880.6	3411.4	12073.6
	washing water	1111.0	6156.0	251.9	0.4	13.6	40.1	12160.0	259.8	965.7	3.2	333.4	1.7		175.0	213.8	1359.0	3784.0	261.7	235.9
8 months	filtered brine	6777.4	33301.1	1407.5	-	167.2	-	60596.3	1658.7	5379.0	-	-	32.3	63.7	1378.2	1071.7	13571.3	24143.6	2418.9	6348.4
	Clear brine	8026.0	39602.7	1665.8	-	194.8	-	76464.3	1959.2	6364.6	-	-	35.2	68.3	1794.0	1340.0	17131.8	28239.0	2986.6	8164.1
	turbid brine	7006.0	34821.2	1469.2	-	180.0	-	68104.4	1726.2	5632.4	-	-	57.3	71.4	1547.9	1195.8	14999.0	25139.0	2674.8	9459.9
	washing water	1153.0	5984.0	232.4	0.2	25.3	54.0	12240.0	278.7	930.5	2.0	155.7	0.9	8.6	193.5	117.3	1092.0	3956.0	308.4	330.9
	leaching water	43.7	228.3	1.1	0.3	-	-	283.8	15.6	3.3	-	-	-	-	-	-	-	11.8	-	-
12 months	filtered brine	11689.1	43706.0	2058.6	-	182.0	-	83230.0	1645.3	8081.1	-	2195.6	-	131.6	2142.7	3160.3	16855.1	55022.0	3284.5	5407.9
	Clear brine	11376.9	42630.0	2007.2	-	183.0	-	83255.5	1567.6	7804.4	-	2068.7	-	138.3	2160.0	3117.3	16954.0	52964.5	3253.6	5995.8
	turbid brine	12102.4	45517.1	2136.6	8.4	209.8	-	87884.4	1703.1	8238.3	-	2305.1	50.8	144.4	2268.8	3379.6	19883.8	56785.5	3512.7	7710.4
	washing water	1497.0	5751.0	251.8	0.4	21.6	-	11820.0	204.0	998.0	-	226.8	-	13.2	223.5	237.6	941.0	6534.0	326.8	169.5
	leaching water	65.8	264.7	2.6	0.4	-	-	615.8	14.8	8.7	-	-	0.5	-	5.4	-	-	45.3	14.7	2.2

Appendix B

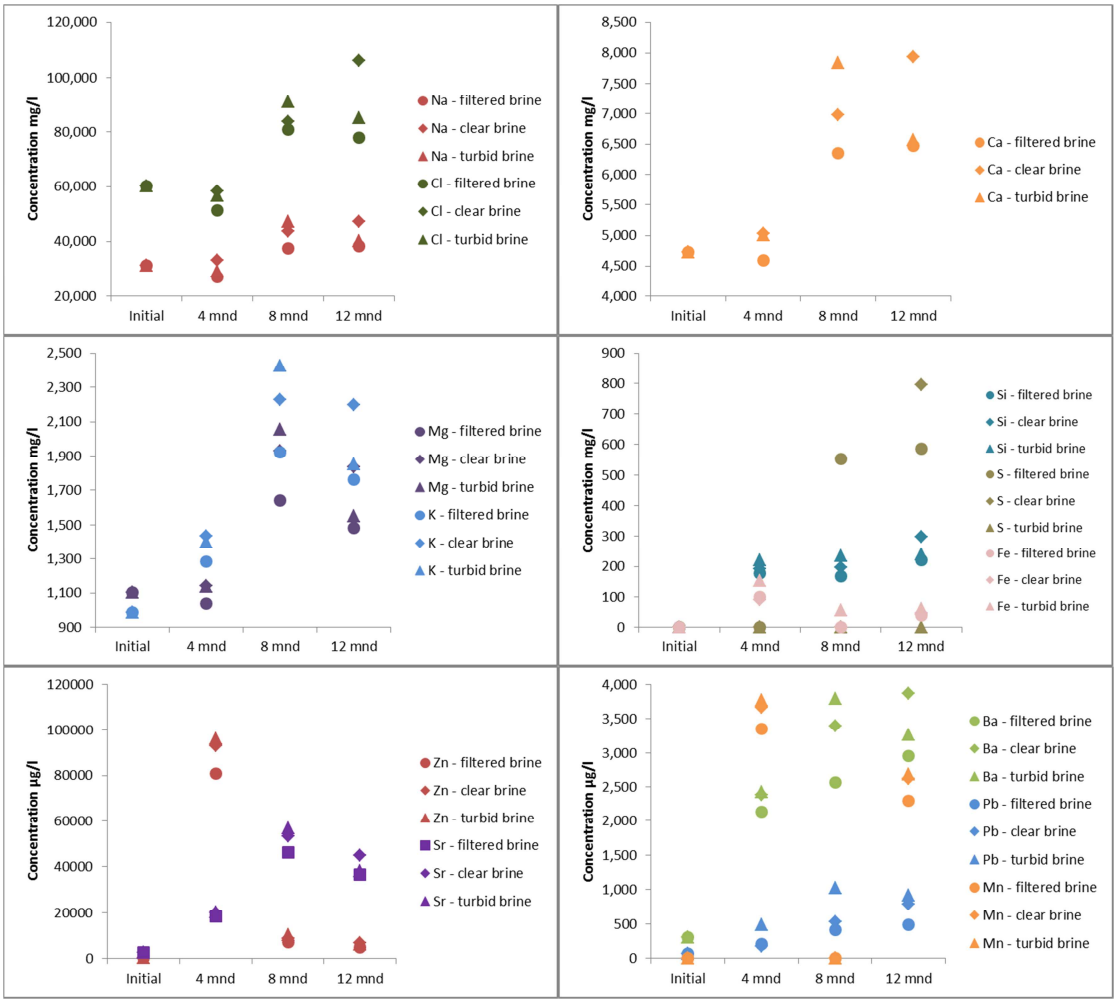

Figure 21. ICP-MS results in time. Note the different scales for the major and trace elements. The elements do not show consistent trends with time. The results for the 4 months experiment have significantly different results.

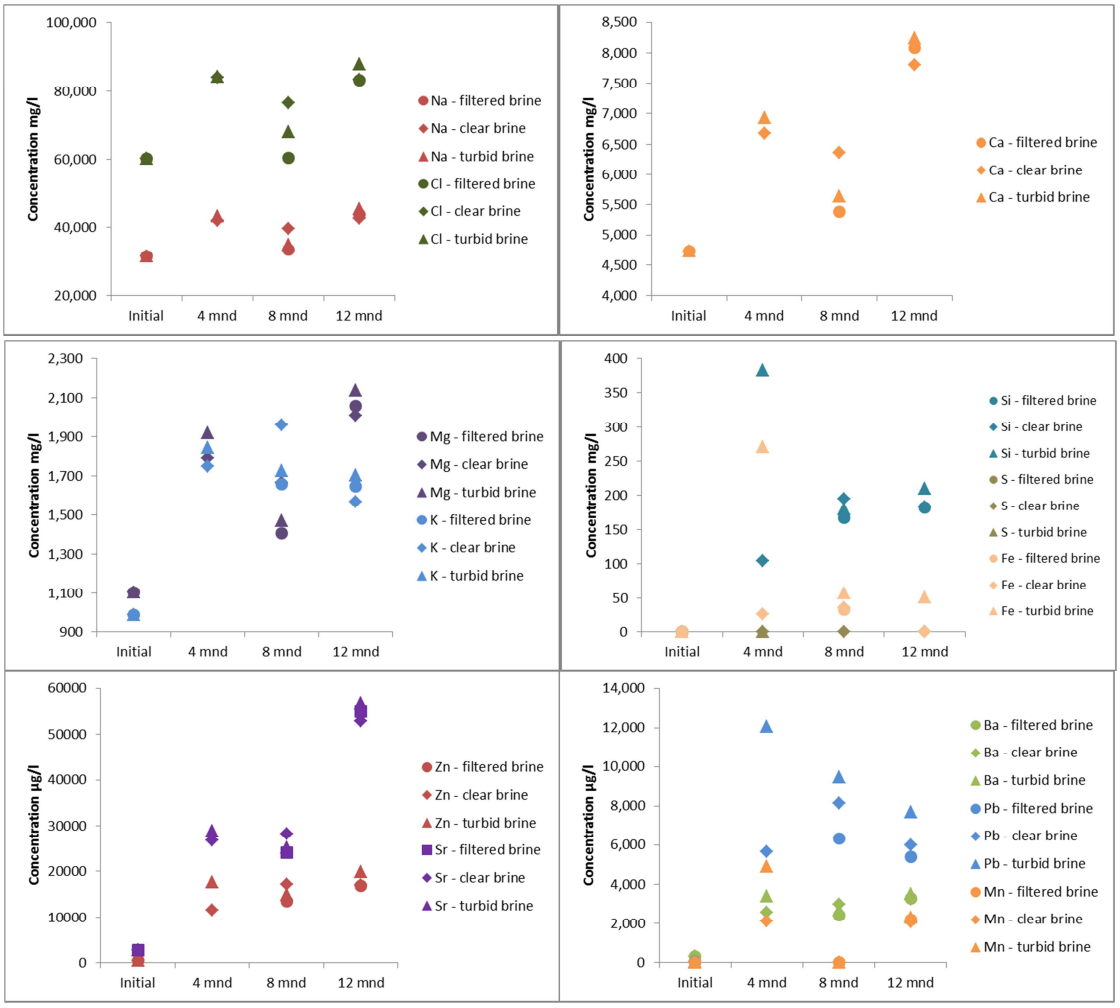

Figure 22. ICP-MS results in time for the caprock experiments. Note the different scales for the major and trace elements. No results are obtained of filtered brine for the 4-months experiment due to insufficient brine.

Appendix C

Table 17. Concentrations from the brine samples divided by the concentrations in the washing water or leaching water for the reservoir experiments. Green: values significantly higher than chlorine (precipitation/adsorption). Pink: values significantly lower than chlorine (additional leaching).

		Li	Na	Mg	Al	Si	S	Cl	K	Ca	Mn	Fe	Co	Ni	Cu	Zn	Sr	Ba	Pb
4 months	filtered brine/washing water	6	6	6	9	7	-	6	6	5	5	10	-	7	7	7	4	12	39
	Clear brine/washing water	6	8	7	13	8	-	7	7	6	6	9	-	8	8	8	5	13	32
	turbid brine/washing water	6	7	6	57	9	-	6	7	6	6	15	-	8	12	9	5	13	90
8 months	filtered brine/washing water	4	4	4	-	4	2	4	4	3	-	-	4	4	4	6	3	6	6
	Clear brine/washing water	4	4	4	-	4	-	4	4	4	-	-	4	4	5	7	4	8	8
	turbid brine/washing water	5	5	5	-	5	-	4	5	4	-	15	5	5	5	8	4	9	15
	filtered brine/leaching water	77	71	80	-	-	6	79	57	40	-	-	70	67	283	147	34	94	-
	Clear brine/leaching water	79	83	94	-	-	-	82	67	44	-	-	81	79	335	179	39	125	-
	turbid brine/leaching water	90	90	100	-	-	-	90	72	50	-	-	88	85	360	208	41	140	-
12 months	filtered brine/washing water	4	4	4	-	4	2	3	4	3	4	5	4	4	4	6	3	7	9
	Clear brine/washing water	5	5	5	-	6	2	5	5	4	4	6	5	6	5	8	4	9	14
	turbid brine/washing water	4	4	4	-	5	-	4	4	3	4	8	4	7	4	7	3	7	17
	filtered brine/leaching water	110	114	128	-	-	3	102	85	23	53	-	79	107	-	-	14	159	-
	Clear brine/leaching water	140	140	159	-	-	4	139	106	29	60	-	104	146	-	-	17	209	-
	turbid brine/leaching water	111	119	134	-	-	-	111	89	24	62	-	89	178	-	-	15	176	-

Table 18. Concentrations from the brine samples divided by the concentrations in the washing water or leaching water for the caprock experiments. Green: values significantly higher than chlorine (precipitation/adsorption). Pink: values significantly lower than chlorine (additional leaching).

		Li	Na	Mg	Al	Si	S	Cl	K	Ca	Mn	Fe	Co	Ni	Cu	Zn	Sr	Ba	Pb
4 months	filtered brine/washing water																		
	Clear brine/washing water	7	7	7	4	8	-	7	7	7	6	15	-	7	10	8	7	10	24
	turbid brine/washing water	7	7	8	339	28	-	7	7	7	15	162	-	11	12	13	8	13	51
8 months	filtered brine/washing water	6	6	6	-	7	-	5	6	6	-	37	7	7	9	12	6	8	19
	Clear brine/washing water	7	7	7	-	8	-	6	7	7	-	41	8	9	11	16	7	10	25
	turbid brine/washing water	6	6	6	-	7	-	6	6	6	-	66	8	8	10	14	6	9	29
	filtered brine/leaching water	155	146	1298	-	-	-	214	106	1640	-	-	-	-	-	-	2055	-	-
	Clear brine/leaching water	184	173	1537	-	-	-	269	126	1940	-	-	-	-	-	-	2403	-	-
	turbid brine/leaching water	160	153	1355	-	-	-	240	111	1717	-	-	-	-	-	-	2139	-	-
12 months	filtered brine/washing water	8	8	8	-	8	-	7	8	8	10	-	10	10	13	18	8	10	32
	Clear brine/washing water	8	7	8	-	8	-	7	8	8	9	-	10	10	13	18	8	10	35
	turbid brine/washing water	8	8	8	22	10	-	7	8	8	10	-	11	10	14	21	9	11	45
	filtered brine/leaching water	178	165	802	-	-	-	135	111	931	-	-	-	400	-	-	1216	224	2460
	Clear brine/leaching water	173	161	782	-	-	-	135	106	899	-	-	-	404	-	-	1170	222	2728
	turbid brine/leaching water	184	172	833	23	-	-	143	115	949	-	98	-	424	-	-	1255	240	3508

Appendix D

Table 19. The measured values divided by the value in the initial brine for the reservoir experiments (upper table) and for the caprock experiments (lower table). The values for Na and Cl are indicative of the evaporation of the brine, resulting in increased Na and Cl concentration. The brine used in the 8 months experiments is from a different batch (second brine batch) than the brine in the 4 and 12 months experiments (first brine batch). The elements which are below detection limit in the initial brine are set at the detection limit. This is true for Al, Si, S, Mn, Fe, Co and Ni in both initial brines. And for Li in the first brine batch and Zn in the second brine batch. This explains the large differences for Li and Zn between the 4 and 12 months and the 8 months experiments.

		Li	Na	Mg	Al	Si	S	Cl	K	Ca	Mn	Fe	Co	Ni	Cu	Zn	Sr	Ba	Pb
4 mnd	filtered brine	4127.1	0.9	0.9	65.2	176.9	-	0.9	1.3	1.0	419.0	1003.2	0.0	19003.1	2.5	154.0	6.6	7.1	3.4
	Clear brine	4472.8	1.1	1.0	94.7	191.6	-	1.0	1.5	1.1	457.7	903.3	0.0	23404.3	2.8	176.7	7.2	7.9	2.8
	Turbid brine	4368.4	0.9	1.0	427.9	221.1	-	0.9	1.4	1.1	471.6	1536.6	0.0	21182.7	4.2	182.7	7.3	8.0	7.9
8 mnd	filtered brine	132.0	1.2	1.5	-	168.4	55.2	1.2	1.4	1.3	-	-	1909.3	1329.7	50.4	906.9	15.9	9.0	11.5
	Clear brine	135.0	1.3	1.8	-	195.6	-	1.2	1.7	1.4	-	-	2208.7	1559.3	59.8	1103.3	18.4	11.9	14.7
	Turbid brine	153.1	1.5	1.9	-	236.4	-	1.3	1.8	1.6	-	558.3	2413.3	1677.7	64.2	1282.1	19.5	13.3	28.5
12 mnd	filtered brine	6961.8	1.2	1.3	-	222.1	58.7	1.3	1.8	1.4	286.7	385.0	2058.1	784.1	6.9	9.5	13.2	9.8	8.0
	Clear brine	8861.8	1.5	1.7	-	298.3	79.6	1.8	2.2	1.7	326.7	453.5	2699.3	1068.2	9.4	12.8	16.2	12.9	12.8
	Turbid brine	7005.6	1.3	1.4	-	241.4	-	1.4	1.9	1.4	335.4	610.3	2322.6	1301.2	7.9	11.6	13.7	10.8	14.9

		Li	Na	Mg	Al	Si	S	Cl	K	Ca	Mn	Fe	Co	Ni	Cu	Zn	Sr	Ba	Pb
4 mnd	filtered brine																		
	Clear brine	19220.3	1.3	1.6	79.2	104.2	0.0	1.4	1.8	1.4	263.9	258.4	0.0	1282.8	10.1	22.0	9.6	8.5	91.8
	Turbid brine	20212.5	1.4	1.7	6913.9	382.9		1.4	1.9	1.5	612.7	2708.7	0.0	1895.3	11.5	33.7	10.4	11.3	196.3
8 mnd	filtered brine	261.6	1.0	1.3	0.0	167.2	0.0	0.9	1.2	1.1	0.0	323.4	636.9	1378.2	20.0	1696.4	8.3	8.5	176.1
	Clear brine	309.8	1.2	1.5	0.0	194.8	0.0	1.1	1.5	1.3	0.0	352.4	683.3	1794.0	25.0	2141.5	9.7	10.5	226.4
	Turbid brine	270.4	1.1	1.4	0.0	180.0	0.0	1.0	1.3	1.1	0.0	573.0	714.4	1547.9	22.3	1874.9	8.7	9.4	262.3
12 mnd	filtered brine	29222.8	1.4	1.9	0.0	182.0	0.0	1.4	1.7	1.7	274.4	0.0	1315.7	2142.7	14.7	32.1	19.9	10.9	87.9
	Clear brine	439.1	1.3	1.9	0.0	183.0	0.0	1.2	1.2	1.6	258.6	0.0	1382.7	2160.0	58.3	2119.3	18.3	11.4	166.3
	Turbid brine	30256.0	1.4	1.9	421.7	209.8	0.0	1.5	1.7	1.7	288.1	507.5	1444.5	2268.8	15.7	37.8	20.5	11.7	125.3

Appendix E

Table 20. Base case equilibrium model results. Minerals in red: not corresponding to experimental results.

	Initial (mol)	Final (mol)	Delta (mol)	Experimental results	Brine concentration	
Albite_low	7.23	0.14	-7.09	Dissolution	Al	4.68E-08
Anhydrite	89.25	88.16	-1.09	Dissolution	C	7.53E-01
Ankerite	6.12	8.90	2.78	?	Ca	2.17E-03
Annite	1.03	0	-1.03	?	Cl	2.37E+00
Dolomite	6.85	5.19	-1.66	Dissolution?	Fe	1.92E-04
Illite_IMt-2	7.07	0.00	-7.07	Precipitation	K	1.22E-01
Kaolinite	8.04	5.10	-2.95	Dissolution	Mg	2.78E-02
Microcline	31.45	37.48	6.03	Possible dissolution	Na	4.23E+00
Muscovite_ord	1.13	1.13	0	?	S	9.81E-01
Quartz,alpha	961.40	956.90	-4.45	Precipitation	Si	1.13E-03
Siderite	10.08	11.39	1.31	Dissolution		
SmectiteMX80_des	0.45	11.67	11.22	Precipitation		

Table 21. Base case equilibrium model results with Illite-Al instead of Illite_IMt-2. Minerals in red: not corresponding to experimental results.

	Initial (mol)	Final (mol)	Delta (mol)	Experimental results	Brine concentration	
Albite_low	7.23	0.00	-7.23	Dissolution	Al	1.05E-08
Anhydrite	89.25	85.49	-3.76	Dissolution	C	6.19E-01
Ankerite	6.12	11.53	5.41	?	Ca	1.47E-03
Annite	1.03	0.00	-1.03	?	Cl	2.28E+00
Dolomite	6.85	5.37	-1.48	Dissolution?	Fe	7.60E-02
Illite_Al	7.07	19.44	12.37	Precipitation	K	5.23E-01
Kaolinite	8.04	0.00	-8.04	Dissolution	Mg	1.83E-02
Microcline	31.45	21.45	-10.00	Possible dissolution	Na	8.64E+00
Muscovite_ord	1.13	1.13	0.00	?	S	3.45E+00
Quartz,alpha	961.40	994.90	33.55	Precipitation	Si	9.45E-04
Siderite	10.08	9.40	-0.68	Dissolution		
SmectiteMX80_des	0.45	0.00	-0.45	Precipitation		

Table 22. Base case equilibrium model results with Illite-Al instead of Illite_IMt-2 and limited albite dissolution. Minerals in red: not corresponding to experimental results.

	Initial (mol)	Final (mol)	Delta (mol)	Experimental results	Brine concentration	
Albite_low	7.23	4.97	-2.26	Dissolution	Al	8.27E-09
Anhydrite	89.25	87.81	-1.44	Dissolution	C	8.03E-01
Ankerite	6.12	8.23	2.11	?	Ca	2.10E-03
Annite	1.03	0.00	-1.03	?	Cl	2.19E+00
Dolomite	6.85	6.36	-0.49	Dissolution?	Fe	7.29E-02
Illite_Al	7.07	17.09	10.02	Precipitation	K	5.30E-01
Kaolinite	8.04	0.00	-8.04	Dissolution	Mg	9.51E-04
Microcline	31.45	23.16	-8.29	Possible dissolution	Na	3.93E+00
Muscovite_ord	1.13	1.13	0.00	?	S	1.10E+00
Quartz,alpha	961.40	982.20	20.89	Precipitation	Si	1.13E-03
Siderite	10.08	11.71	1.63	Dissolution		
SmectiteMX80_des	0.45	0.00	-0.45	Precipitation		

Table 23. Base case equilibrium model results with Illite-Al instead of Illite_IMt-2, limited albite dissolution and secondary magnesite. Minerals in red: not corresponding to experimental results.

	Initial (mol)	Final (mol)	Delta (mol)	Experimental results	Brine concentration	
Albite_low	7.23	4.97	-2.26	Dissolution	Al	8.27E-09
Anhydrite	89.25	88.00	-1.25	Dissolution	C	8.03E-01
Ankerite	6.12	14.39	8.27	?	Ca	2.10E-03
Annite	1.03	0.00	-1.03	?	Cl	2.19E+00
Dolomite	6.85	0.00	-6.85	Dissolution?	Fe	7.29E-02
Illite_Al	7.07	16.97	9.90	Precipitation	K	5.30E-01
Kaolinite	8.04	0.00	-8.04	Dissolution	Mg	9.51E-04
Magnesite(Natur)	0.00	4.54	4.54		Na	3.93E+00
Microcline	31.45	23.51	-7.94	Possible dissolution	S	1.10E+00
Muscovite_ord	1.13	1.13	0.00	?	Si	1.13E-03
Quartz,alpha	961.40	981.60	20.21	Precipitation		
Siderite	10.08	7.40	-2.68	Dissolution		
SmectiteMX80_des	0.45	0.00	-0.45	Precipitation		

Table 24. Base case equilibrium model results with Illite-Al instead of Illite_IMt-2, limited albite dissolution, no dolomite dissolution and secondary calcite. Minerals in red: not corresponding to experimental results.

	Initial (mol)	Final (mol)	Delta (mol)	Experimental results	Brine concentration	
Albite_low	2.26	0.00	-2.26	Dissolution	Al	1.18E-08
Anhydrite	89.25	88.22	-1.03	Dissolution	C	9.35E-01
Ankerite	6.12	6.68	0.56	?	Ca	2.42E-03
Annite	1.03	0.00	-1.03	?	Cl	2.18E+00
Calcite	0.00	0.65	0.65	?	Fe	7.28E-02
Dolomite	6.85	6.85	0.00	Dissolution?	K	2.98E-01
Illite_Al	7.07	16.83	9.77	Precipitation	Mg	4.77E-06
Kaolinite	8.04	0.00	-8.04	Dissolution	Na	3.92E+00
Microcline	31.45	23.89	-7.56	Possible dissolution	S	9.10E-01
Muscovite_ord	1.13	1.13	0.00	?	Si	1.13E-03
Quartz,alpha	961.40	980.80	19.50	Precipitation		

Siderite	10.08	12.80	2.72	Dissolution
SmectiteMX80_des	0.45	0.00	-0.45	Precipitation

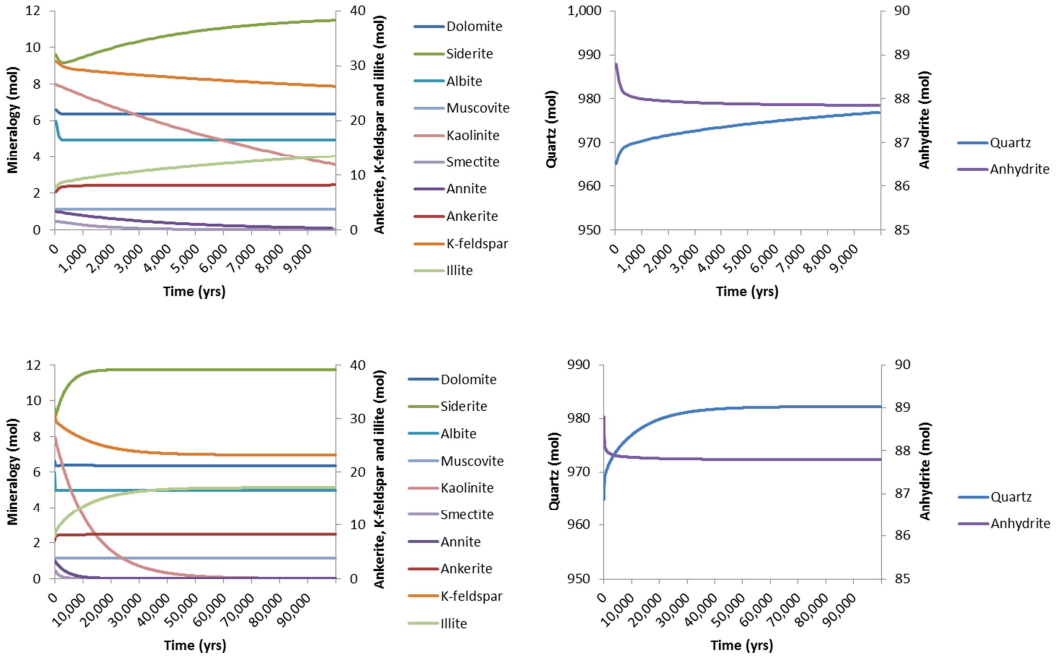

Figure 23. Mineral reactions in time, predicted by the model with limited albite dissolution. Note that each graph has two y-axes.

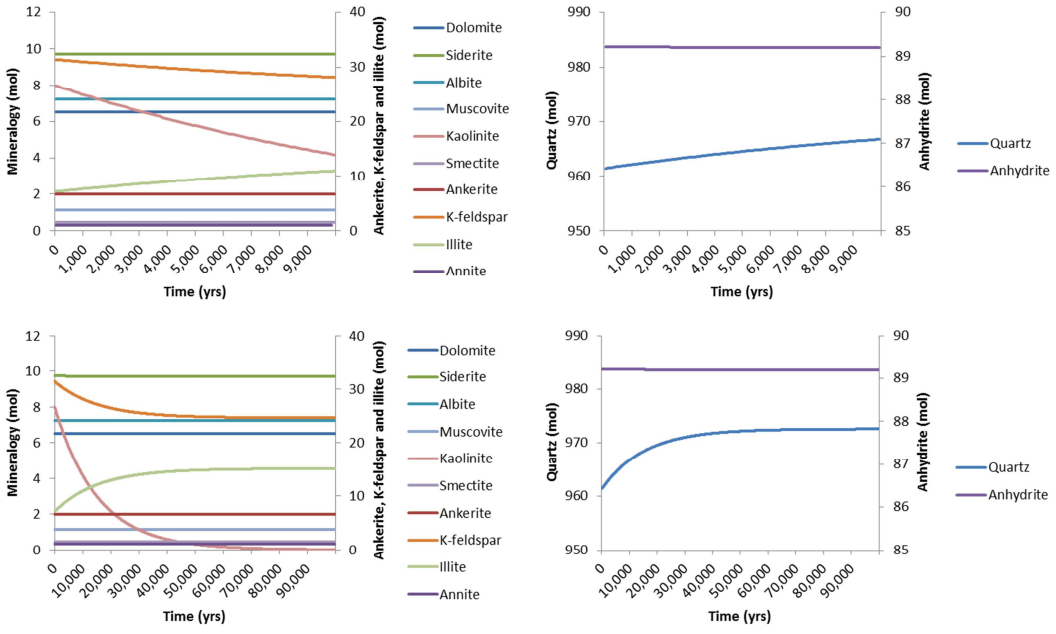

Figure 24. Mineral reactions in time, predicted by the kinetic base case model without CO_2. Note that each graph has two y-axes.

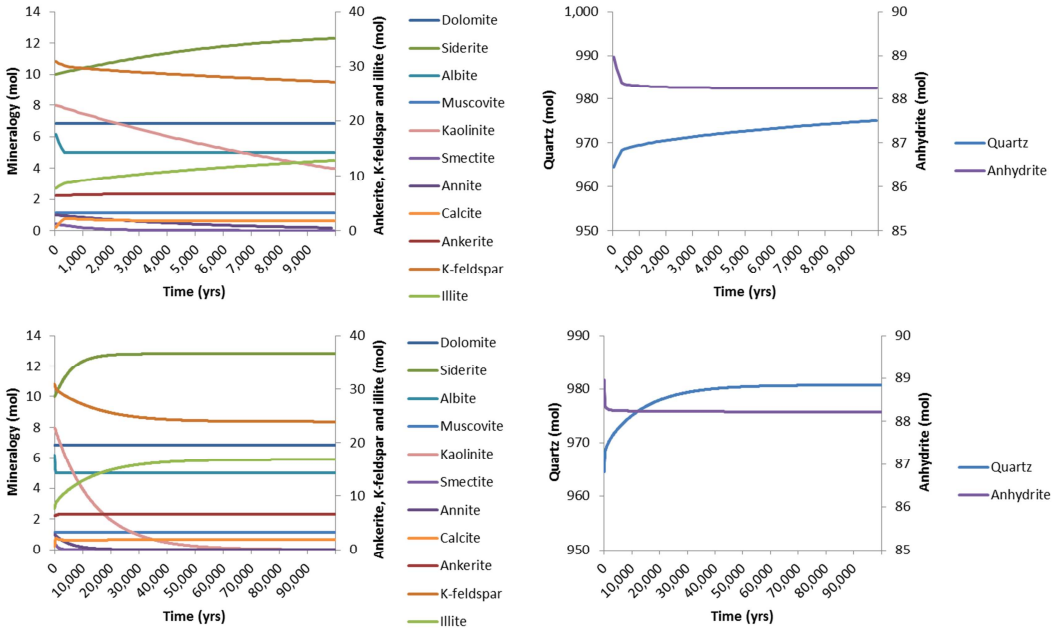

Figure 25. Mineral reactions in time, predicted by the kinetic model without dolomite dissolution. Note that each graph has two y-axes.

Appendix F

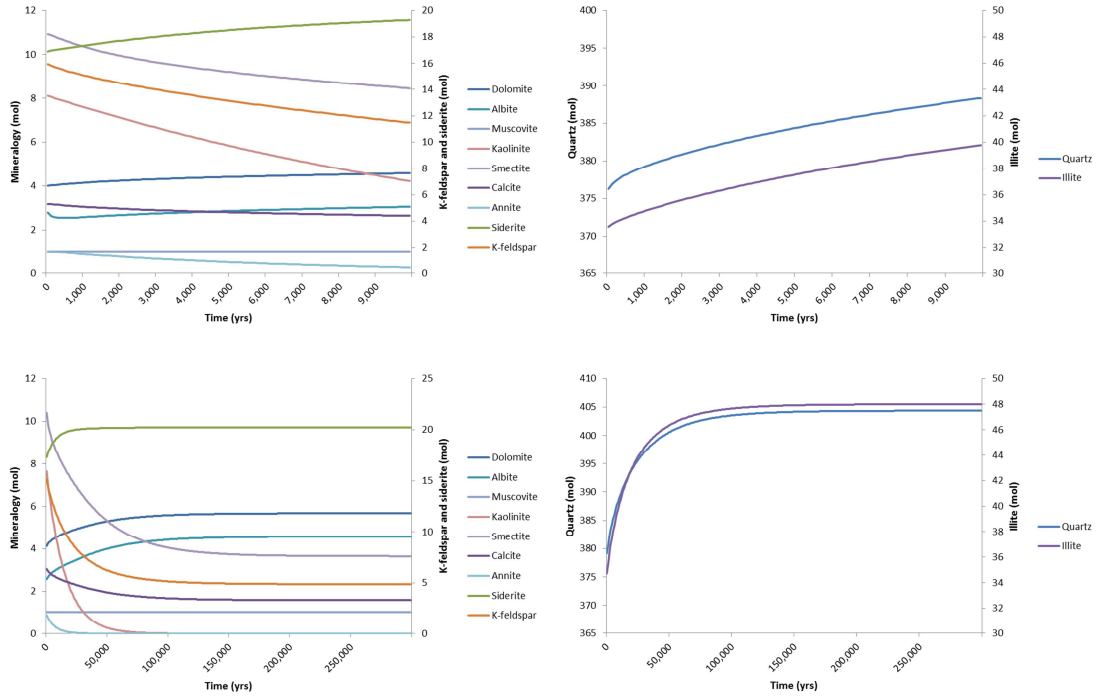

Figure 26. Mineral reactions in time for the caprock up to 10,000 years (upper) and 300,000 years (lower) for the CO_2 model without primary ankerite. Note that each graph has two y-axes.

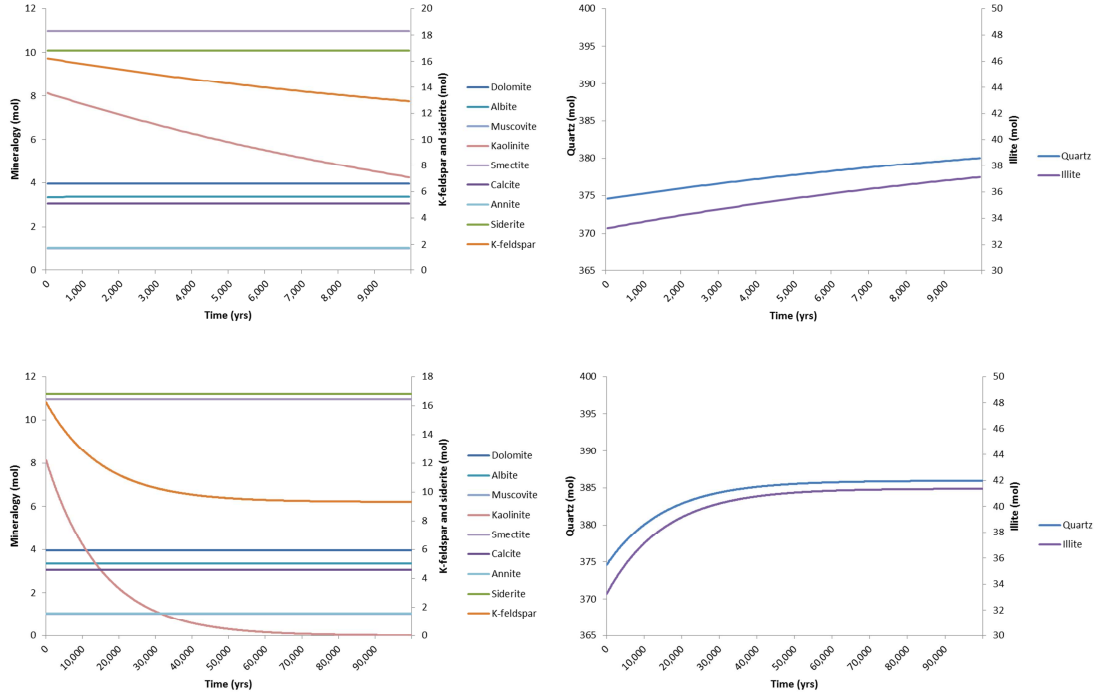

Figure 27. Mineral reactions in time for the caprock up to 10,000 years (upper) and 100,000 years (lower) for the reference model. Note that each graph has two y-axes.

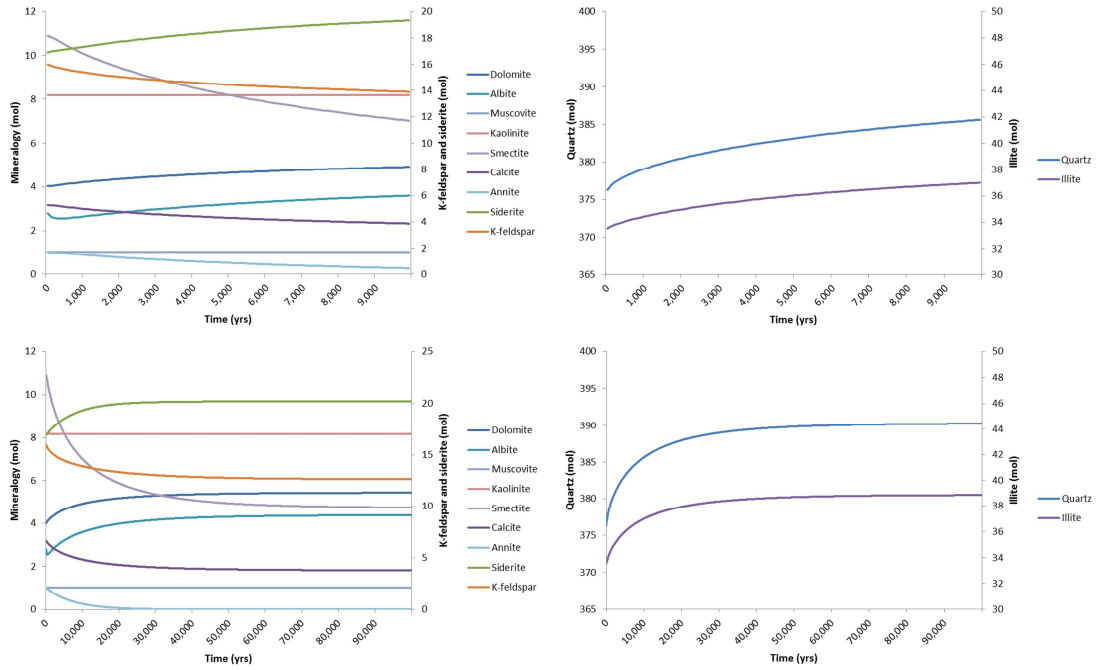

Figure 28. Mineral reactions in time for the caprock up to 10,000 years (upper) and 100,000 years (lower) for the CO_2 model excluding kaolinite dissolution. Note that each graph has two y-axes.